Publications of the Astronomical Society of Australia (PASA), Vol. 33, e054, 20 pages (2016).

doi:10.1017/pasa.2016.46

Observational Signatures of High-Redshift Quasars and Local Relics of Black Hole Seeds

Amy E. Reines[1,3*] and Andrea Comastri[2]

[1]National Optical Astronomy Observatory, 950 North Cherry Avenue, Tucson, AZ 85719, USA
[2]INAF - Osservatorio Astronomico di Bologna, via Ranzani 1, 40127, Bologna, Italy
[3]Email: reines@noao.edu

(Received April 29, 2016; Accepted September 2, 2016)

Abstract

Observational constraints on the birth and early evolution of massive black holes come from two extreme regimes. At high redshift, quasars signal the rapid growth of billion-solar-mass black holes and indicate that these objects began remarkably heavy and/or accreted mass at rates above the Eddington limit. At low redshift, the smallest nuclear black holes known are found in dwarf galaxies and provide the most concrete limits on the mass of black hole seeds. Here, we review current observational work in these fields that together are critical for our understanding of the origin of massive black holes in the Universe.

Keywords: black hole physics – galaxies: active – galaxies: dwarf – quasars: general – surveys

1 INTRODUCTION

One of the major outstanding issues in modern astrophysics is how the first 'seeds' of supermassive black holes (BHs) formed at high redshift. BHs with masses exceeding $M_{\rm BH} \gtrsim 10^9 {\rm M}_\odot$ power the most luminous quasars that have been discovered near the edge of the observable Universe, the record holder being ULAS1120+0641 at $z = 7.085$ (Mortlock et al. 2011). The very presence of such massive objects less than a Gyr after the Big Bang poses serious challenges for models of their formation and subsequent evolution (i.e., Volonteri 2010; Johnson & Haardt 2016; Latif & Ferrara 2016).

Proposed theories for the formation of BH seeds include remnants from the first generation of massive stars (e.g., Population III stars, Madau & Rees 2001; Haiman & Loeb 2001), where intermittent episodes of super-Eddington accretion could grow these seeds of $\sim$100 M$_\odot$ into $\sim 10^9$ M$_\odot$ BHs within several hundred Myr (Madau, Haardt, & Dotti 2014, also see, for example, Wyithe & Loeb 2012; Alexander & Natarajan 2014; Volonteri, Silk, & Dubus 2015 for possible conditions leading to super-Eddington accretion onto BHs at high redshift). Alternatively, BH seeds may have been significantly more massive, formed from the rapid inflow and subsequent collapse of gas (e.g., Loeb & Rasio 1994; Begelman, Volonteri, & Rees 2006; Lodato & Natarajan 2006; Choi, Shlosman, & Begelman 2015) or from collisions in dense star clusters (e.g., Portegies Zwart et al. 2004; Devecchi & Volonteri 2009; Davies, Miller, & Bellovary 2011; Lupi et al. 2014; Stone, Kuepper, & Ostriker 2016). Starting with a more massive seed (e.g., $M_{\rm BH} \sim 10^5 {\rm M}_\odot$) in models of BH growth eases the problem of assembling enough luminous $\sim 10^9$ M$_\odot$ BHs by redshifts $z \sim 6-7$ under the assumption of Eddington-limited accretion (e.g., Natarajan & Volonteri 2012; Hirschmann et al. 2012).

At present, directly observing the first high-redshift BH seeds is not feasible. Various studies have looked for AGN signatures in early galaxies at redshifts $z \gtrsim 5$, but they are not detected even in the deepest X-ray observations (e.g., Willott 2011; Cowie, Barger, & Hasinger 2012; Treister et al. 2013; Weigel et al. 2015; Vito et al. 2016). Recently, however, a few 'direct collapse' BH candidates with $M_{\rm BH} \sim 10^5 - 10^6 {\rm M}_\odot$ at $z \gtrsim 6$ have been proposed (Pacucci et al. 2016) including the extremely luminous Lyα emitter CR7 (Sobral et al. 2015; Pallottini et al. 2015; Hartwig et al. 2016; Agarwal et al. 2016; Smith et al. 2016; Smidt, Wiggins, & Johnson 2016), although see Bowler et al. (2016) for more standard interpretations of the data. In any case, our knowledge of high-redshift BHs is primarily limited to luminous quasars with hefty BHs ($M_{\rm BH} \gtrsim 10^8 - 10^9 {\rm M}_\odot$).

A complementary approach to learn about BH seeds is to search for the smallest nuclear BHs ($M_{\rm BH} \lesssim 10^5 {\rm M}_\odot$) in present-day dwarf galaxies, which provides the most direct observational constraints on seed masses (for earlier reviews,

[*] Hubble Fellow

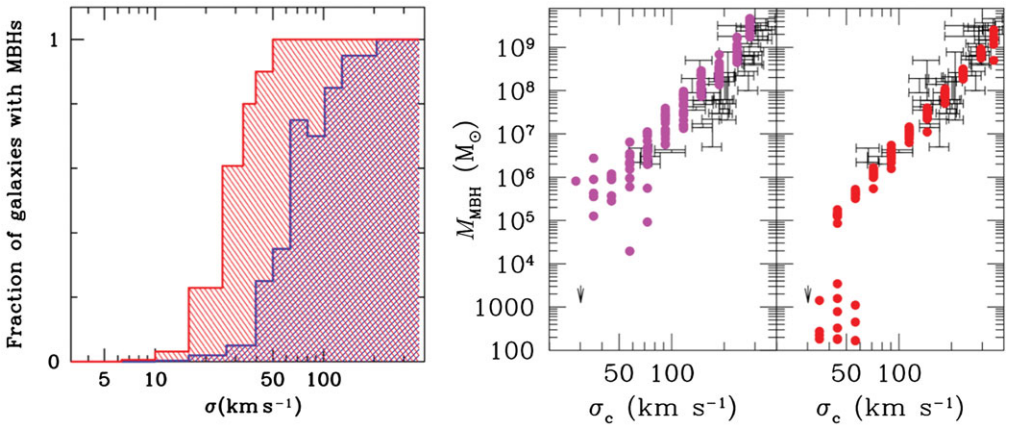

Figure 1. Predictions at $z = 0$ from the models of Volonteri, Lodato, & Natarajan (2008b) and van Wassenhove et al. (2010) provide diagnostics for distinguishing between BH seed formation mechanisms. The observational signatures of BH seeds are strongest in dwarf galaxies. Left: BH occupation fraction as a function of velocity dispersion for light seeds (remnants from Pop III stars; red) and heavy seeds (direct collapse; purple). Courtesy of M. Volonteri. Right: $M_{\rm BH} - \sigma$ relation at $z = 0$ starting with heavy (purple, left panel) and light (red, right panel) seeds. Observational data (black points) are from Tremaine et al. (2002). Adapted from Volonteri et al. (2008a).

see Volonteri 2010 and Greene 2012). Unlike massive galaxies with BHs that have grown substantially through accretion and mergers, dwarf galaxies that have experienced significantly calmer merger histories may host BHs that are relatively pristine.

Indeed, models of BH growth in a cosmological context indicate that the observational signatures indicative of seed formation are strongest in dwarf galaxies (Volonteri et al. 2008b; Volonteri & Natarajan 2009; van Wassenhove et al. 2010; Bellovary et al. 2011; Habouzit, Volonteri, & Dubois 2016). The primary diagnostics at $z \sim 0$ include the BH occupation fraction, the distribution of BH masses, and BH-host galaxy scaling relations at low mass (for a review, see Volonteri 2010). Figure 1 shows predictions from Volonteri et al. (2008b) and van Wassenhove et al. (2010). At high velocity dispersions (and high masses), the BH occupation fraction is equal to 1 regardless of the initial seeds. Likewise, the $M_{\rm BH} - \sigma$ relation is indistinguishable for the different seeding scenarios at the high-mass end. These results can be understood as the result of numerous mergers and accretion episodes resulting in the build-up of massive galaxies and their BHs. From Figure 1, we can see that the picture is entirely different in the low-mass regime. Some early galaxies will have quietly coasted through cosmic time without getting assembled into a massive galaxy, thereby retaining some 'memory' of the initial seeding conditions. The fraction of these galaxies that host a massive BH today will reflect the fraction of galaxies that hosted a massive BH at early times, where the expectation is a high occupation fraction in the case of light seeds (Pop III remnants) and a low occupation fraction in the case of heavy seeds (direct collapse). Predictions for the $M_{\rm BH} - \sigma$ relation at $z \sim 0$ are also distinct at the low-mass end due to the different mass distributions of relatively ungrown BHs.

Until recently, very few dwarf galaxies had *observational* evidence for hosting massive BHs ($M_{\rm BH} \sim 10^4 - 10^6 M_\odot$) and these objects were thought to be extremely rare. In the past decade, the field has undergone rapid growth and we have gone from a handful of prototypical examples (e.g., NGC 4395; Filippenko & Sargent 1989, and Pox 52; Kunth, Sargent, & Bothun 1987) to large systematically assembled samples demonstrating that massive BHs in low-mass galaxies are much more common than previously thought (e.g., Greene & Ho 2004; Reines, Greene, & Geha 2013).

Here, we review current observational studies that inform our understanding of the birth and early growth of massive BHs. This review has two main parts. In Section 2, we review observations of high-redshift BHs, with an emphasis on optical/near-infrared and X–ray surveys of the quasar population. In Section 3, we review searches for local relics of BH seeds in dwarf galaxies. We conclude in Section 4 with a discussion of how these observations are constraining models for the formation of the first seed BHs.

2 OBSERVATIONAL SIGNATURES OF HIGH-REDSHIFT QUASARS

The quasar spectral energy distribution (SED) covers a broad range of wavelengths. Quasars emit almost constant power per unit decade from the far-infrared to the hard X-ray band. The bolometric energy of a quasar peaks in the optical/UV which, at high redshift, is shifted to the near-infrared. A significant fraction of the total nuclear emission is in the X-ray band. Optical to near-infrared and X-ray surveys thus represent the most efficient way to select large, relatively unbiased samples of quasars over a large redshift range and especially at the greatest distances.

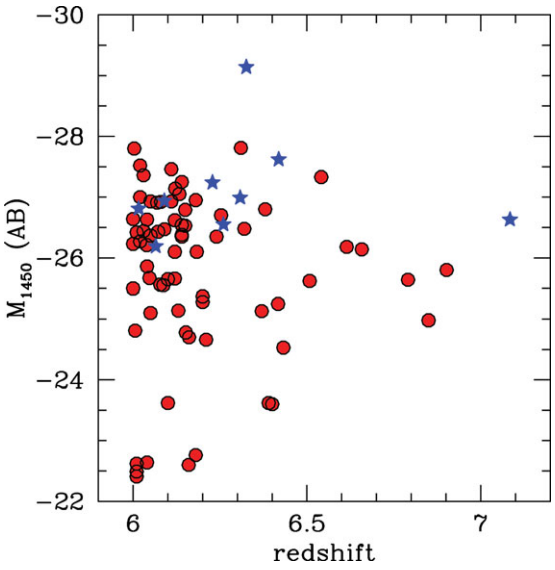

Figure 2. Rest frame UV luminosity (M_{1450}) versus redshift for the sample of the $z > 6$ quasars currently known in the literature mainly from the Calura et al. (2014) compilation, complemented by the results published in Venemans et al. (2013), Venemans et al. (2015), Bañados et al. (2014), Carnall et al. (2015), Kashikawa et al. (2015), Wu et al. (2015), Reed et al. (2015), Matsuoka et al. (2016), and Bañados et al. (2016). The blues stars represent objects detected in the X-ray band either in pointed observations or as serendipitous sources in the field of view of different targets.

2.1. Optical and near-IR surveys

A quantum leap forward in the search for and the study of the primeval quasars has been obtained primarily by the Sloan Digital Sky Survey (SDSS, Fan et al. 2001), complemented by the Canada–France High-Redshift Survey (CFHQS), the Pan STARRS survey (PSO, Kaiser et al. 2002), the UKIDSS (Lawrence et al. 2007) Large Area Survey (ULAS), the VISTA VIKING (Edge et al. 2013), and VST ATLAS (Shanks et al. 2015) surveys. More recently, the first results from the Dark Energy Survey (DES, Reed et al. 2015), the Subaru Suprime Cam surveys (Kashikawa et al. 2015), and the Hyper Suprime Cam (HSC) survey (Matsuoka et al. 2016) were published, and there are newly identified quasars from the Pan-STARRS1 survey (Bañados et al. 2016). At the time of writing, the most up to date compilation of optically selected quasars at $z > 6$ includes ~ 80 objects and these are listed in Table 1. Their rest-frame UV luminosity versus redshift is shown in Figure 2. Roughly 10% of these are also detected in the X-ray band in follow-up or snapshot pointings.

From a visual inspection of Figure 2, it is evident that, with the exception of a few objects, only the bright-end tail of the luminosity distribution is currently sampled. A major step forward is expected by the current and foreseen HSC surveys that have already started to dig into the low-luminosity tail of the distribution (Matsuoka et al. 2016), and by the upcoming LSST survey that is designed to have the required depth and wavelength coverage to detect a large number of quasars at $z \sim 7$. The number density of QSOs brighter than $M_{1450} = -26.7$ is of the order of one object per Gpc^3 at $z \sim 6$ (see Fan 2012 for a review) and thus large areas must be surveyed to a depth which is sufficient to find a sizable number of objects. Such a trade off is currently feasible only in the optical/near-infrared.

The space density peaks at $z \sim 2$–3, which is known as the quasar era or 'cosmic noon'. Before and after the peak, the number density decreases sharply. The exponential decline at $z > 3$ was noted since the first optical surveys (Schmidt, Schneider, & Gunn 1995) and now is put on solid grounds. The comoving density of $z \sim 6$ quasars is almost two orders of magnitude lower than that at the $z \sim 2$–3 peak.

The bright end of the QSO luminosity function from the 6 000 deg^2 SDSS survey was extended to lower luminosities ($M_{1450} \sim -24$ at $z \sim 5$) by McGreer et al. (2013). The data reach below the break in the luminosity function at those redshifts ($M^*_{1450} \sim -27$). The decrease in the density of luminous ($M^*_{1450} \sim -26$) QSOs is more pronounced, by about a factor 2, going from $z = 5$ to $z = 6$ than from $z = 4$ to $z = 5$. Whilst the precise shape of the decline in the space density of luminous QSOs towards high redshift is debated, there is no doubt that they experienced a rapid evolution from the primeval Universe to cosmic noon.

The evolution rate and the shape of the luminosity function at lower luminosities are much more uncertain due to the lack of sensitive enough observations. An attempt to push the high-z QSO census towards low luminosities is presented in Ikeda et al. (2011) and Glikman et al. (2011). They measured the luminosity function down to $M_{1450} \sim -22$, but cannot push beyond $z \sim 4$. A summary of the shape of the QSO space density as a function of luminosity over the entire redshift range is shown in Figure 3 from Ikeda et al. (2011). The decline towards high redshifts can be reliably measured only for high luminosity QSOs. At low luminosities, the results are dominated by large uncertainties. Recently, however, Giallongo et al. (2015) has pushed to even lower luminosities. They find 22 AGN candidates at $z > 4$ in the CANDELS GOODS-South field, and estimate the UV luminosity function in the absolute magnitude interval $-22.5 \lesssim M_{1450} \lesssim -18.5$ and the redshift interval $4 < z < 6.5$.

The first supermassive BHs are expected to grow via gas accretion and mergers of smaller mass seed BHs (see Johnson & Haardt 2016 this volume). The mergers of galaxies hosting BHs are also likely to trigger gas accretion and make them luminous optical and X-ray sources. If this were the case, high-z QSOs are expected to reside in galaxy overdense regions enhancing the probability of finding lower luminosity active supermassive BHs in their vicinity. A search for galaxy overdensities at high redshift over a relatively large area, using the Subaru Suprime Cam is reported by Utsumi et al. (2010) and recently extended by Morselli et al. (2014) around the fields of four high-z ($\sim$6) QSOs with the Large Binocular Camera camera on the Large Binocular Telescope (LBT). Deep photometric images were obtained in the r-, i-, and z-bands down to a 50% completeness limit of $z_{AB} \sim 25$ (see Figure 4). Candidate high-z dropouts were selected

Table 1. The $z > 6$ quasar sample

Name	RA	Dec	M_{1450}	z	Reference	Discovery Survey
J0009+3252	00 09 30.89	+32 52 12.94	−25.65	6.10	Ban16	PanSTARRS1
J0028+0457	00 28 06.56	+04 57 25.64	−26.64	6.00	Ban16	PanSTARRS1
J0033−0125	00 33 11.40	−01 25 24.9	−25.02	6.13	Wil07	CFHT_RCS2
J0050+3445	00 50 06.67	+34 45 22.6	−28.43	6.25	Wil10	CFHT_RCS2
J0055+0146	00 55 02.91	+01 46 18.3	−24.95	6.02	Wil09	CFHT_RCS2
J0100+2802	01 00 13.20	+28 02 25.8	−29.26	6.30	Wu15	SDSS_boss
J0109−3047	01 09 53.13	−30 47 26.3	−25.55	6.745	Ven13	VIKING
J0136+0226	01 36 03.17	+02 26 05.7	−24.78	6.21	Wil10	CFHT_RCS2
J0142−3327	01 42 43.70	−33 27 45.7	−27.8	6.31	Car15	VST/ATLAS
J0159−3633	01 59 57.95	−36 33 56.9	−27.0	6.02	Car15	VST/ATLAS
J0210−0456	02 10 13.19	−04 56 20.9	−24.31	6.44	Wil10b	CFHT_W1
J0216−0455	02 16 27.81	−04 55 34.1	−22.62	6.01	Wil09	CFXT_SXDS
J0221−0802	02 21 22.71	−08 02 51.5	−24.83	6.16	Wil10	CFHT_W1
J0226+0302	02 26 01.88	+03 02 59.4	−27.36	6.53	Ven15	PanStarrs
J0227−0605	02 27 43.33	−06 05 31.4	−25.41	6.20	Wil09	CFHT_W1
J0231−2850	02 31 52.96	−28 50 20.08	−26.23	6.0	Ban14	PanSTARRS1
J0303−0019	03 03 31.40	−00 19 12.9	−25.50	6.07	Jia08	SDSS_S82
J0305−3150	03 05 16.92	−31 50 56.0	−25.99	6.60	Ven13	VIKING
J0353+0104	03 53 49.72	+01 04 04.4	−26.56	6.05	Jia08	SDSS_S82
J0402+2451	04 02 12.69	+24 51 24.43	−26.95	6.18	Ban16	PanSTARRS1
J0421−2657	04 21 38.05	−26 57 15.61	−27.25	6.14	Ban16	PanSTARRS1
J0422−1927	04 22 01.00	−19 27 28.69	−26.62	6.12	Ban16	PanSTARRS1
J0454−4448	04 54 01.79	−44 48 31.1	−26.48	6.09	Reed15	DES
J0559−1535	05 59 45.47	−15 35 00.20	−26.93	6.05	Ban16	PanSTARRS1
J0818+1722	08 18 27.40	+17 22 51.8	−27.43	6.00	Fan06	SDSS_main
J0828+2633	08 28 13.41	+26 33 55.49	−26.37	6.05	War	UKIDSS
J0842+1218	08 42 29.00	+12 18 50.5	−27.21	6.08	DeR11	SDSS_main
J0859+0022	08 59 07.19	+00 22 55.9	−23.56	6.39	Mat16	HyperSuprimeCam
J1030+0524	10 30 27.10	+05 24 55.0	−27.18	6.28	Fan01	SDSS_main
J1036−0232	10 36 54.19	−02 32 37.94	−26.80	6.38	Ban16	PanSTARRS1
J1048+4637	10 48 45.05	+46 37 18.3	−27.58	6.23	Fan03	SDSS_main
J1110−1329	11 10 33.98	−13 29 45.6	−25.58	6.51	Ven15	PanStarrs
J1120+0641	11 20 01.48	+06 41 24.3	−26.63	7.08	Mor11	UKIDSS
J1137+3549	11 37 17.73	+35 49 56.9	−27.14	6.01	Fan06	SDSS_main
J1148+0702	11 48 03.29	+07 02 08.3	−25.81	6.29	War14	UKIDSS
J1148+5251	11 48 16.64	+52 51 50.3	−27.85	6.43	Fan03	SDSS_main
J1152+0055	11 52 21.27	+00 55 36.6	−24.91	6.37	Mat16	HyperSuprimeCam
J1205−0000	12 05 05:09	−00 00 27.9	−24.19	6.85	Mat16	HyperSuprimeCam
J1207−0005	12 07 54.14	−00 05 53.3	−22.57	6.01	Mat16	HyperSuprimeCam
J1207+0630	12 07 37.44	+06 30 10.2	−26.34	6.04	Ban14	UKIDSS
J1217+0131	12 17 21.34	+01 31 42.47	−25.37	6.20	Ban16	PanSTARRS1
J1250+3130	12 50 51.93	+31 30 21.9	−27.16	6.13	Fan06	SDSS_main
J1257+6349	12 57 57.48	+63 49 37.16	−26.27	6.02	Jia15	SDSS_overlap
J1306+0356	13 06 08.27	+03 56 26.36	−26.81	6.02	Fan01	SDSS_main
J1319+0950	13 19 11.29	+09 50 51.4	−27.15	6.13	Mor09	UKIDSS
J1401+2749	14 01 47.34	+27 49 35.03	−26.54	6.14	Ban16	PanSTARRS1
J1402+4024	14 02 54.67	+40 24 03.19	−25.86	6.04	Ban16	PanSTARRS1
J1427+3312	14 27 38.59	+33 12 42.0	−26.47	6.12	McG06	NDWFS
J1428−1602	14 28 21.39	−16 02 43.30	−26.93	6.11	Ban16	PanSTARRS1
J1429+5447	14 29 52.17	+54 47 17.7	−25.88	6.21	Wil10	CFHT_W3
J1431−0724	14 31 40.45	−07 24 43.47	−26.35	6.14	Ban16	PanSTARRS1
J1509−1749	15 09 41.78	−17 49 26.8	−26.98	6.12	Wil07	CFHT_VW
J1558−0724	15 58 50.99	−07 24 43.47	−27.46	6.11	Ban16	PanSTARRS1
J1602+4228	16 02 53.98	+42 28 24.9	−26.92	6.07	Fan04	SDSS_main
J1603+5510	16 03 49.07	+55 10 32.3	−22.58	6.04	Kas15	SuprimeCAM
J1609+3041	16 09 37.27	+30 41 47.78	−26.38	6.14	War	UKIDSS
J1623+3112	16 23 31.81	+31 12 00.5	−26.69	6.22	Fan04	SDSS_main
J1630+4012	16 30 33.90	+40 12 09.6	−26.14	6.05	Fan03	SDSS_main
J1641+3755	16 41 21.64	+37 55 20.5	−25.48	6.04	Wil07	CFHT_RCS2
J1932+7139	19 32 07.62	+71 39 08.41	−26.92	6.08	Ban16	PanSTARRS1
J2032−2114	20 32 09.99	−21 14 02.31	−26.35	6.24	Ban16	PanSTARRS1

Table 1. Continued.

Name	RA	Dec	M_{1450}	z	Reference	Discovery Survey
J2054-0005	20 54 06.49	−00 05 14.8	−26.18	6.06	Jia08	SDSS_S82
J2100−1715	21 00 54.62	−17 15 22.5	−25.42	6.09	Wil10	CFHT_VW
J2215+2606	22 15 56.63	+26 06 29.41	−26.44	6.03	Ban16	PanSTARRS1
J2216−0016	22 16 44.47	−00 16 50.1	−23.56	6.10	Mat16	HyperSuprimeCam
J2219+0102	22 19 17.22	+01 02 48.9	−23.10	6.16	Kas15	SuprimeCAM
J2228+0128	22 28 27.83	+01 28 09.5	−22.36	6.01	Mat16	HyperSuprimeCam
J2229+1457	22 29 01.65	+14 57 09.0	−24.91	6.15	Wil10	CFHT_VW
J2232+0012	22 32 12.03	+00 12 38.4	−22.70	6.18	Mat16	HyperSuprimeCam
J2232+2930	22 32 55.15	+29 30 32.2	−26.04	6.66	Ven15	PanStarrs
J2236+0032	22 36 44.58	+00 32 56.9	−23.55	6.40	Mat16	HyperSuprimeCam
J2240−1839	22 40 48.98	−18 39 43.8	−26.49	6.00	Ban14	PS1
J2310+1855	23 10 38.88	+18 55 19.7	−27.47	6.00	Wan13	SDSS_main
J2315−0023	23 15 46.57	−00 23 58.1	−25.46	6.12	Jia08	SDSS_S82
J2318−0246	23 18 02.80	−02 46 34.0	−25.23	6.05	Wil09	CFHT_RCS2
J2329−0301	23 29 08.28	−03 01 58.8	−25.23	6.43	Wil07	CFHT_RCS2
J2348−3054	23 48 33.34	−30 54 10.0	−25.75	6.886	Ven13	VIKING
J2356−0622	23 56 32.45	−06 22 59.26	−26.79	6.15	Ban16	PanSTARRS1
J2356+0023	23 56 51.58	+00 23 33.3	−25.00	6.00	Jia09	SDSS_S82

Columns 1–5: Names, coordinates, UV luminosities and redshifts for the sample of quasars plotted in Figure 2. Column 6: References. Wil07/09/10/10b=Willott et al. (2007, 2009, 2010a, 2010b), Fan01/03/04/06= Fan et al. (2001, 2003, 2004, 2006), Ven13/15= Venemans et al. (2013, 2015), Car15=Carnall et al. (2015), Jia08/09=Jiang et al. (2008, 2009), Reed15=Reed et al. (2015), DeR11=De Rosa et al. (2011), Mat16=Matsuoka et al. (2016), Mort09/11=Mortlock et al. (2009, 2011), Kas15=Kashikawa et al. (2015), Ban14/16=Banados et al. (2014, 2016), Wan13=Wang et al. (2013), Wu15=Wu et al. (2015), War=Warren et al. (in preparation). Column 7: The discovery surveys and/or instruments, as discussed in the main text.

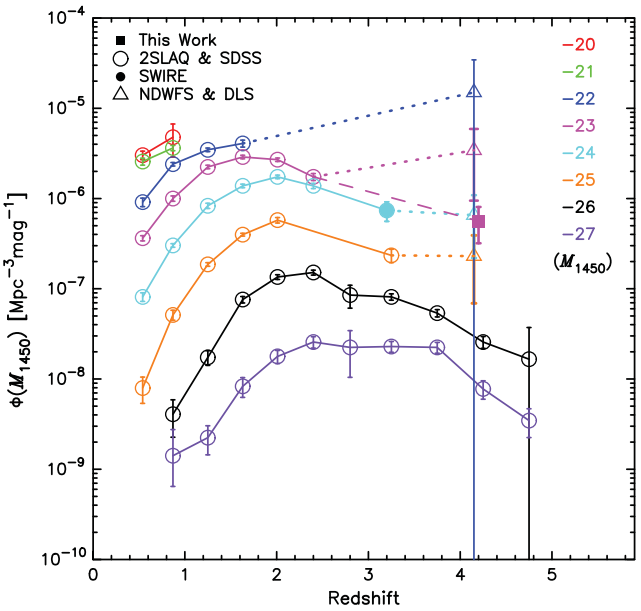

Figure 3. Redshift evolution of the quasar space density. Coloured lines indicate different values of M_{1450}. Dotted lines show the combined 2dF-SDSS Luminous Red Galaxies and Quasar Survey (2SLAQ), SDSS, the Spitzer wide area infrared extragalactic legacy survey (SWIRE), the NOAO Deep and Wide Field Survey (NDWFS), and the Deep Lens Survey (DLS). Dashed line shows the combined COSMOS and 2SLAQ QLF. From Ikeda et al. (2011). © AAS. Reproduced with permission.

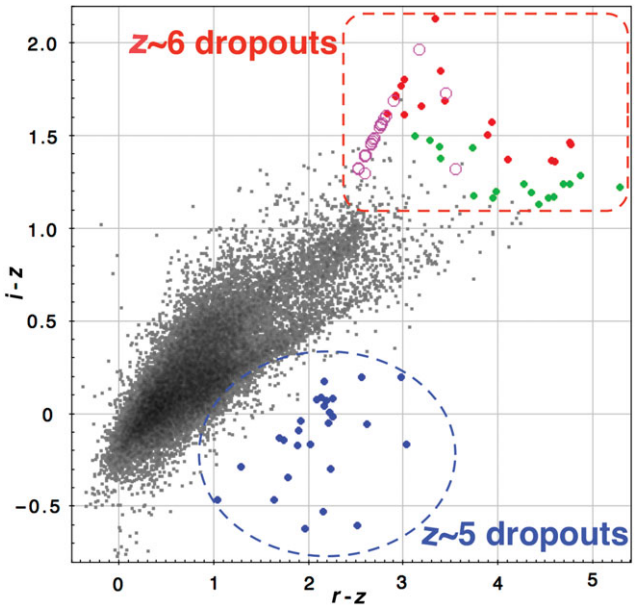

Figure 4. i–z versus r–z diagram for the LBC sources in J1030 field (small gray dots; ≈30 000 objects). LBC primary and secondary i-dropouts are shown as red- and green-filled circles, respectively. Magenta dots are even fainter i-dropouts ($25.2 < z_{AB} < 25.5$) All the i-dropout highlighted in the upper right part of the plot are undetected in the deep r-band ($r \sim 27.5$) LBT image. The LBC $z \sim 5$ galaxy candidates are shown as blue dots.

using a conservative $i - z > 1.4$ threshold. The results indicate that the spatial density of dropouts is higher than expected in a 'blank' field at the $\sim 3.7\sigma$ level. An intensive programme of follow-up spectroscopic observations is currently underway with the LUCI spectrograph on the LBT. A recently approved *Chandra* Large Program (P.I. R. Gilli) will enable the association of high-z candidates with faint AGN emitting in the X-ray band.

Despite strong cosmological evolution, active BHs show a self-similar behaviour for other properties such as the optical/near-infrared continuum and the emission line intensities. Also, the X-ray spectra are almost indistinguishable over the entire $z \sim 0$–7 redshift range. The detection of metal emission lines redward of Lyα suggests that rapid chemical enrichment has occurred. The mid- to far-infrared emission indicates the presence of hot dust heated from the nuclear radiation. The lack of significant changes along cosmic history, in the above described observables, challenges the physical interpretation and the models for the evolution of accreting supermassive BHs. A few departures from the self-similar behaviour were reported by Jiang et al. (2010) in terms of a lack of mid-infrared emission, associated to hot dust, in two $z \sim 6$ quasars. The two objects lie in the low tail of the BH mass distribution of QSOs at $z \sim 6$, and could represent an early phase of evolution when the BH is growing and the dust is not yet produced.

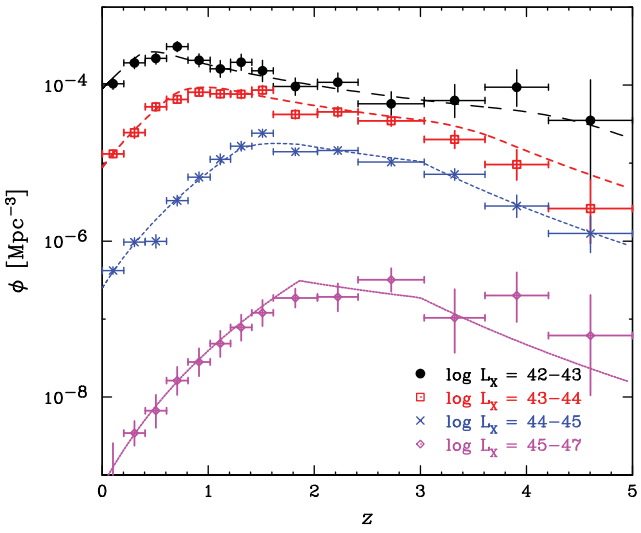

Figure 5. The space density of X-ray selected AGN for different luminosity bins as labelled. The peak progressively moves to lower redshifts as the luminosity decreases. From Ueda et al. (2014). © AAS. Reproduced with permission.

2.2. X-ray surveys

The above described population of optically luminous QSOs hosting supermassive BHs ($M_{\rm BH} > 10^9 M_\odot$) at $z > 6$, likely represents the tip of the iceberg of the luminosity and mass functions. According to theoretical models for structure formation, massive BHs ($M_{\rm BH} \sim 10^4$–10^7 $M_\odot$) are predicted to be abundant in the early Universe. Moreover, it is well known that the majority of the accretion power, recorded in the spectrum of the X-ray background, is obscured by large amounts of gas and dust. The space density and the cosmological evolution of X-ray selected AGN is now relatively well understood, thanks to the large number of surveys performed with XMM-*Newton*, *Chandra*, and *NuSTAR*, built upon previous observations with ROSAT, ASCA, BeppoSAX, Swift-BAT, and INTEGRAL. The evolution of the luminosity function is computed on samples of a few thousand objects over a broad range of X-ray luminosities ($\sim 10^{42}$–10^{46} erg s^{-1}) and up to redshifts 3–4 (e.g., Ueda et al. 2014; Miyaji et al. 2015; Buchner et al. 2015; Aird et al. 2015). The evolution of X-ray selected AGN including obscured objects, except the deeply buried Compton thick AGN, is described by a luminosity-dependent model and shown in Figures 5 and 6. The peak in the space density is at higher redshifts for higher luminosity objects, an effect known as downsizing that also describes the evolution of star-forming galaxies. The X-ray luminosity function and the evolution of obscured AGNs is accurately described by phenomenological models such as the Luminosity Dependent Density Evolution (LDDE) or the Flexible Double Power Law (FDPL) up to $z \sim 3$–4. Both LDDE and FDPL suggest a complex luminosity dependence in the redshift evolution, possibly associated to the accretion rate. Irrespective of the adopted parameterisation, the space density exponentially decreases up to $z \sim 5$. At higher redshifts, the amplitude and the shape of the decline in the QSO space density is not well constrained.

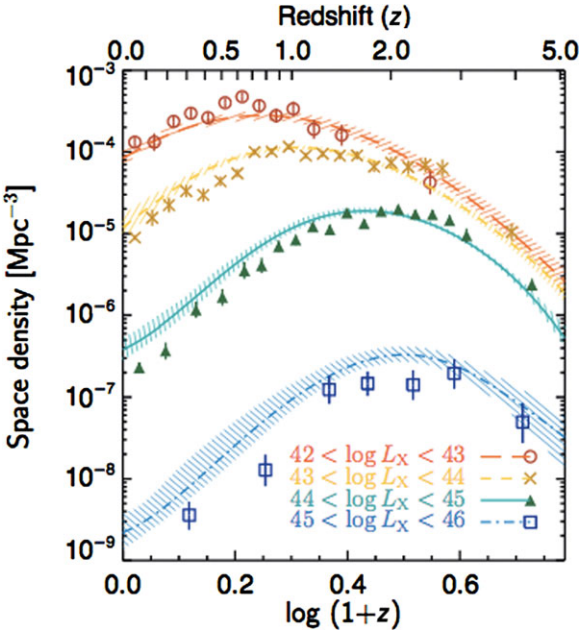

Figure 6. The same as for Figure 5 but from Figure 18 in Aird et al. (2015).

In order to improve our understanding of BH growth and of AGN triggering mechanisms in the early Universe, it is necessary to increase the statistics of the AGN population at $z > 3$. In the last decade, observations obtained with XMM-*Newton* and *Chandra* were sensitive enough to investigate the high-redshift Universe in the X-ray band. Two pioneering works were performed in the 2 deg^2 COSMOS field, using XMM-*Newton* (Brusa et al. 2009 $N_{z>3} = 40$), and *Chandra*, on the central 0.9 deg^2 (Civano et al. 2011, $N_{z>3} = 81$), reaching a luminosity limit of $L_{2-10\rm keV} = 10^{44.2}$ erg s^{-1} and $L_{2-10\rm keV} = 10^{43.55}$ erg s^{-1}, respectively. Vito et al. (2013) were able

to extend their analysis down to $L_{2-10\mathrm{keV}} \simeq 10^{43}$ erg s^{-1}, using the 4 Ms *Chandra* Deep Field South (CDF-S, Xue et al. 2011) catalogue ($N_{z>3} = 34$); the same group (Vito et al. 2014) studied the 2–10 keV luminosity function in the redshift range $z = [3–5]$, combining deep and shallow surveys ($N_{z>3} = 141$). Kalfountzou et al. (2014) combined the C-COSMOS sample with the one from the wide and shallow ChaMP survey (Kim et al. 2007; Green et al. 2009; Trichas et al. 2012) to have a sample of 211 objects at $z > 3$ and 27 at $z > 4$, down to a luminosity $L_{2-10\mathrm{keV}} = 10^{43.55}$ erg s^{-1}. All these works show a decline of the AGN space density at $z > 3$, but they are not able to put significantly better constraints at $z > 4$, due to still poor statistics. Moreover, when combining different surveys, one has to assume completeness corrections, therefore introducing uncertainties in the final results.

Recently, Georgakakis et al. (2015) combined data from different surveys to obtain a sample of 340 sources at $z > 3$ over about three orders of magnitude, $L_{2-10\mathrm{keV}} \simeq [10^{43}–10^{46}]$ erg s^{-1}, whilst Marchesi et al. (2016b) collect 174 objects at $z \geq 3$ in the 2 deg^2 *Chandra Legacy* survey (Marchesi et al. 2016a; Civano et al. 2016). The former is the largest sample of X-ray selected $z > 3$ AGN so far published, whilst the latter is that with the highest spectroscopic redshift completeness (50%). Both of them agree on the fact that the number density of high-z QSOs exponentially decrease in the redshift range $z \sim 3–5$; moreover, it is suggested that the evolution of the luminous ($> 10^{45}$ erg s^{-1}) QSOs is milder than that of lower luminosity objects. Marchesi et al. (2016b) also point out that at luminosities larger than 10^{44} erg s^{-1}, the ratio between obscured and unobscured AGN at $z \sim 5$ is larger by a factor 2 than that observed at $z \sim 3–4$.

An improved determination of the shape of the bright end of the X-ray luminosity function is expected from the currently ongoing large area X-ray surveys in SDSS Stripe82 (LaMassa et al. 2016) and XXL (Pierre et al. 2016). They are approaching a sky coverage of the order of 100 deg^2 in the soft X-ray band and will act as pathfinders of the forthcoming all sky *eROSITA* X-ray survey (Merloni et al. 2012).

A different approach with respect to the blind X-ray detection adopted in the above described works is pursued in Fiore et al. (2012a). The search for X-ray emission from high-redshift AGNs in the CDF-S is performed using a specifically developed X-ray detection technique, optimised for faint sources, and further assisted by the analysis of deep optical and near-infrared images. They evaluated the comoving space density of faint X-ray sources at $z > 3$ with a sample of 40 sources. In the highest redshift bin $z > 5.8$ (and corresponding X-ray luminosities $> 10^{43.5}$ erg s^{-1}), there are only two sources. The estimated space density of $\sim 6.6 \times 10^{-6}$ Mpc^{-3} is likely to be an upper limit. It is concluded that the slope of the faint end of the luminosity function is much flatter than the bright end. The characteristic luminosity L^* evolves rapidly and the density of X-ray selected AGN decreases by more than a factor 3 from $z \sim 3$ to $z \sim 6$. The above described technique is further elaborated by Giallongo et al. (2015) with the aim to estimate the AGN UV emissivity and their contribution to the reionisation of the Universe. The main conclusion of their analysis is that AGN may play a relevant role in the reionisation of the Universe at $z > 6$. The large uncertainty in the data and the paucity of $z > 6$ sources in the sample call for the need of larger samples and deeper data.

More recently, Cappelluti et al. (2016) employed a similar procedure based on the prior knowledge of the position of the optical counterpart of ∼35 000 CANDELS sources selected in the *H*-band in the deepest area of the *Chandra* 4 Ms observations. This technique led to a significant increase in the number of X-ray detections down to a limiting flux of $\sim 10^{-17}$ erg cm^{-2} s^{-1}. Also, in this case, there are no clear examples of X-ray sources at very high redshifts. Moreover, the number of candidate high-z AGN in Cappelluti et al. (2016) is lower, by about a factor 2, than that reported in Giallongo et al. (2015).

Another systematic search for X-ray selected AGN at $z >$ 5–6 is presented by Weigel et al. (2015). They started from a sample of X-ray confirmed sources in the 4 Ms CDF-S and employed a variety of tools to assess the robustness of the high-z sample (visual classification, colour criteria, X-ray hardness ratios, and a redetermination of the best fit photo-z). They conclude that only a few, possibly none, of the high-z candidates survived after the analysis suggesting that the space density of $z > 5$ X-ray selected AGN drops even faster than previously reported. The dearth of X-ray emitting AGNs at high redshift is confirmed by the X-ray stacking analysis of the 4 Ms *Chandra* data at the position of colour-selected $z \sim 6$, 7, and 8 CANDELS galaxy candidates (Treister et al. 2013). The upper limits on the average X-ray luminosities are of the order of 10^{42-43} erg s^{-1} in the hard X-ray band.

A further deep search for X-ray emission from high redshift galaxies in the CDF-S using the 7 Ms data (Luo et al., in preparation) was recently performed by Vito et al. (2016), stacking the data at the positions of more than 2 000 optically selected galaxies. They find that the stacked X-ray emission in galaxies at $z \sim 4–5$ is likely dominated by processes related to star formation. Mass accretion onto SMBHs in individually X-ray-undetected galaxies is negligible, compared with the BH accretion rate density measured for samples of X-ray detected AGN. The ultradeep limiting flux is achieved only on a small portion of the field of view of the order of a few arcminutes, highlighting the need of larger area surveys to uncover high-redshift SMBHs.

The bottom line is that the current number of X-ray selected AGN at very high redshift ($z > 6$) is consistent with zero. There might be a few candidates, but either the redshift determination is uncertain or the source could be a spurious detection in X-rays or both. Much deeper X-ray observations will certainly help to obtain additional and tighter constraints on the emissivity of high-redshift AGN.

2.3. ATHENA surveys

The detection of large, statistically meaningful samples of QSOs around and below the L^* luminosity at $z > 6$, and over

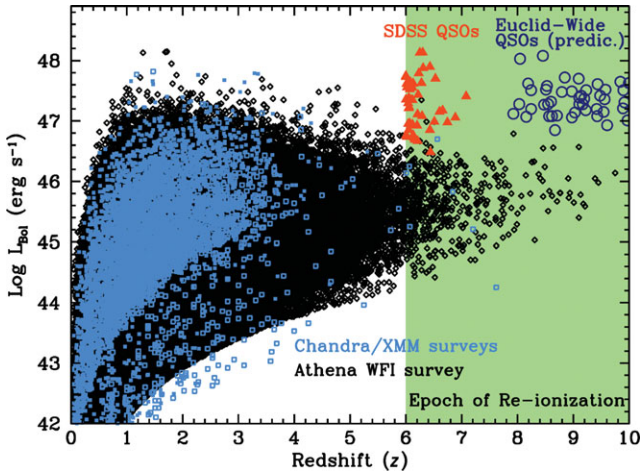

Figure 7. The luminosity-redshift plane of representative X-ray and optical surveys as labelled. The blue squares are the sources detected in current X-ray surveys. Data are from the COSMOS-Legacy survey and the *Chandra* Deep Field South. Filled squares represent sources with a spectroscopic redshift, whilst empty squares have photo-z's. The red triangles are the SDSS QSOs reported in Figure 2. The open empty blue circles are the predictions for the Euclid surveys (Roche et al. 2012). The black diamonds are the predictions from the large and deep Athena surveys (Aird et al. 2013).

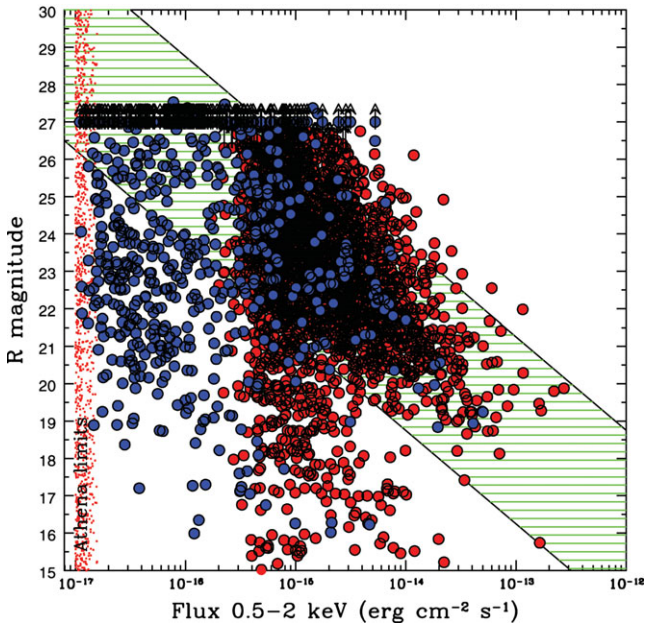

Figure 8. The observed R magnitudes of X-ray source optical counterparts in the XMM and *Chandra* COSMOS survey (red dots) and in the CDF-S 4 Ms exposure (blue dots). Optically undetected sources are reported with arrows. The area enclosed between the two diagonal lines corresponds to X-ray to optical flux ratios typical of X-ray selected AGN. Optical bright, X-ray faint sources in the lower left part of the diagram are mainly low-luminosity AGNs and star-forming galaxies. The *ATHENA* limits are indicated by small red squares. High-redshift AGNs are expected to be extremely faint or undetectable in the optical bands, depending on redshift.

a wide range of obscuring column densities, would provide unique constraints on the formation and early growth of BHs. This will require a next generation of X-ray observatories that can perform surveys to comparable depths as the deepest *Chandra* fields, but over a substantially larger areas. The *ATHENA* X-ray observatory (Nandra et al. 2013), currently approved as an ESA large mission for a launch in 2028, has the capability to probe this new discovery space.

The prospects for a multi-tiered *ATHENA* Wide Field Imaging survey, combining extremely deep and shallower wide area observations, include the ability to identify a statistically meaningful sample of AGNs at very high ($z > 6$) redshifts and thereby revolutionise our understanding of the early Universe at the epoch of reionisation (Aird et al. 2013). The multi-cone *ATHENA* Wide Field Imager (WFI) survey has been designed to maximise the instrument capabilities and the expected breakthroughs in the determination of the luminosity function and its evolution at high (>4) and very high (>6) redshifts. It is a major investment of the entire science programme and will take more than 1 yr of observations.

To adequately constrain the faint end of the luminosity function ($L \sim 10^{43-44}$ erg s^{-1} at $z \sim 6$–8) requires a survey that reaches flux limits of $\sim 3 \times 10^{-17}$ erg s^{-1} cm^{-2} over an area a few square degrees and of $\sim 2 \times 10^{-16}$ erg s^{-1} cm^{-2} over several tens of square degrees. This coverage is well beyond the capability of current X-ray observatories. The expected output of the multitiered *Athena* WFI survey is shown in Figure 7 over the entire range of redshifts, and well within the epoch of the reionisation (i.e., up to $z \sim 10$). From a visual inspection, it is clear that X-ray surveys will nicely complement current and future optical and near-infrared surveys sampling the low-luminosity tail of the distribution.

Even though the *ATHENA* multi-cone survey has been designed to detect several hundreds (>400, at $z > 6$) of AGN minimising the obscuration biases, a full multi-wavelength approach that combines world-class ground-based facilities and space-based missions is needed to understand the physics of the early evolutionary stages. The search for optical and near-infrared counterparts of the *ATHENA* X-ray sources will require the survey of large sky areas, from a few up to several tens of square degrees, down to faint and ultra-faint magnitudes. The typical magnitudes of the optical counterparts of large samples of *Chandra* and XMM sources in the COSMOS and CDF-S fields are shown in Figure 8. The LSST-Deep and Euclid-Deep fields (reaching AB magnitudes ∼28 and ∼26 in the optical and near-infrared, respectively, over 40 deg^2), are well matched to the various layers of the *ATHENA* surveys. For the faintest X-ray sources, the superior capabilities (near-infrared AB magnitude limit of about 30) of the *James Webb Space Telescope (JWST)* will be needed.

Accurate redshift measurements will be provided by near-infrared spectroscopic follow-up from the planned European Extremely Large Telescope (E-ELT), which will deliver superb spectroscopic capabilities down to $H_{AB} \sim 29$. The cold dust content and the molecular gas dynamics of the faint obscured AGN will be measured by the ALMA interferometer, mainly using the [CII] 158 μm line (Pentericci et al. 2016). The Square Kilometer Array (SKA) will detect radio

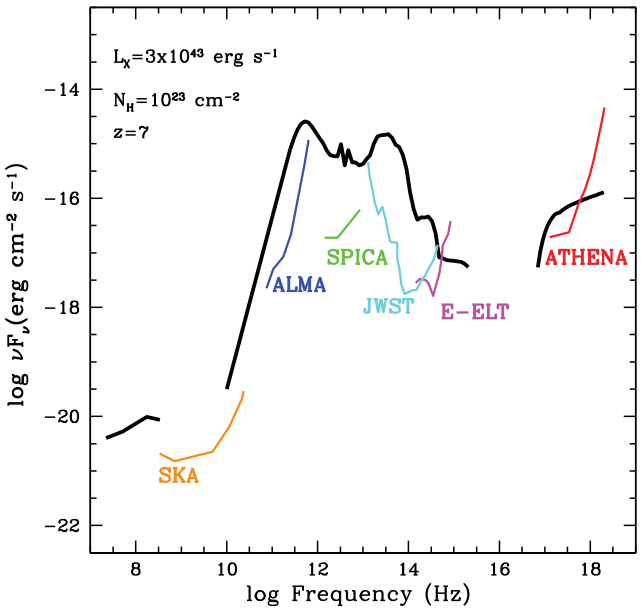

Figure 9. Broadband SED of a moderate-luminosity obscured AGN (as labelled) at $z = 7$, which will be observable in the *ATHENA* surveys. The thick black line is that of an obscured AGN with similar luminosity and obscuring column density in the COSMOS survey (Lusso et al. 2011) redshifted to $z = 7$. The 3σ sensitivities (for a typical survey exposure) of SKA, ALMA, SPICA, JWST, and E-ELT are also shown, as labelled (Aird et al. 2013).

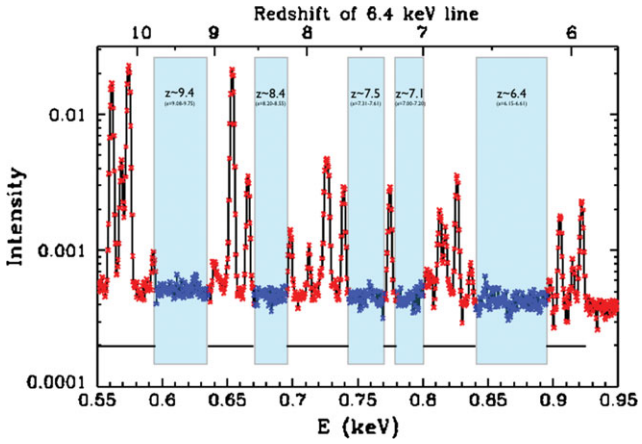

Figure 10. The instrumental background free windows in the XIFU detector where a highly redshifted (as labelled), iron Kα could be detected. Simulations show that an ultra-deep 1 Ms exposure could reveal heavily obscured line dominated sources at $z \sim 8$.

emission amongst a sizable fraction of high-z obscured AGN. It is interesting to note that at the time of the *ATHENA* surveys, both SKA and E-ELT should be fully operational. In Figure 9, the SED of an obscured AGN at $z = 7$ is shown along with the sensitivities of major multi-wavelength observatories.

Finally, *ATHENA* may be able to reveal the presence of heavily obscured, accreting supermassive BHs within samples of high-z galaxies that remain beyond the spectroscopic capabilities of E-ELT. Deep observations with the X-ray Integral Field Unit (XIFU) would provide ultra-deep, high-resolution X-ray spectroscopy and may directly measure the redshift of deeply buried, Compton thick AGNs at $z > 8$ if a strong 6.4 keV (rest-frame) Fe Kα emission line is detected (see Figure 10). The detection of such a line would place constraints on the metallicity and could thus constrain the star-formation history of the host galaxy.

By sampling moderate to low-luminosity AGNs, *ATHENA* will start to probe the BH mass function towards values of $M_{\rm BH} \sim 10^{6-7}{\rm M}_\odot$, depending on accretion rate. This will help pave the way for detailed studies of accretion physics over a broad range of BH and host galaxy masses and luminosities. The X-ray Surveyor, a large mission concept that is currently being studied for the next Decadal Survey in the United States, would be sensitive to fainter X-ray fluxes than *ATHENA* due to the sub-arcsec spatial resolution. This would enable the BH mass function at high redshift to be probed to even lower masses, ultimately providing tighter constraints on BH seeds.

3 LOCAL RELICS OF BLACK HOLE SEEDS IN DWARF GALAXIES

As discussed above, the detection of the first high-redshift BH seeds is beyond our current capabilities and will continue to be challenging even with the next generation of ground- and space-based observatories. However, present-day dwarf galaxies, which have low masses and relatively quiet merger histories, offer another avenue to observationally constrain the origin of massive BHs. Searching for the smallest nuclear BHs in today's dwarf galaxies ($M_{\rm BH} \lesssim 10^5{\rm M}_\odot$) and studying their properties can place valuable constraints on the masses, host galaxies, and even the formation mechanism of BH seeds (Volonteri 2010; Greene 2012).

3.1. Dynamical searches

In general, the most reliable method for discovering massive BHs and measuring their masses is to use stellar or gas dynamics to weigh the central BH (for a review, see Kormendy & Ho 2013). There are a few detections and upper limits on dynamical BH masses in nearby dwarf galaxies, and these are summarised in Table 2[1]. However, at present, dynamical searches are quite limited since the gravitational sphere of influence cannot be resolved for low-mass BHs in dwarf galaxies much beyond the Local Group. Consider, for example, a $10^5{\rm M}_\odot$ BH in a dwarf galaxy with a stellar velocity dispersion of $\sigma = 30$ km s^{-1}. The radius of influence in this case is only $\sim$0.5 pc (where $r_{\rm infl} = GM_{\rm BH}/\sigma^2$). Future large ($\sim$30 m) ground-based telescopes will expand the volume in which we can use dynamical methods to search for massive BHs in dwarf galaxies, but for now, we are forced to look for accreting BHs shining as AGNs in populations of more distant dwarf galaxies.

[1] Also, see Gebhardt et al. (2001), Barth et al. (2009), and Neumayer & Walcher (2012) for BH mass upper limits in late-type spiral galaxies.

PASA, 33, e054 (2016)
doi:10.1017/pasa.2016.46

Table 2. BH masses and upper limits in nearby dwarf galaxies based on stellar and gas dynamics.

Galaxy	Description	$M_{\rm BH}$	Reference
M32	elliptical, M31 satellite	$(2.4 \pm 1.0) \times 10^6$	van den Bosch & de Zeeuw (2010)[a]
NGC 404	S0, $d \sim 3.06$ Mpc	$4.5^{+3.5}_{-2.0} \times 10^5$	Seth et al. (2010)
NGC 4395	Sd, $d \sim 4.4$ Mpc	$4^{+8}_{-3} \times 10^5$	den Brok et al. (2015)
NGC 205	elliptical, M31 satellite	$\leq 2.2 \times 10^4$	Valluri et al. (2005)
Fornax	spheroidal, MW satellite	$\leq 3.2 \times 10^4$	Jardel & Gebhardt (2012)
Ursa Minor	spheroidal, MW satellite	$\leq (2-3) \times 10^4$	Lora et al. (2009)

[a]Also see e.g., Dressler & Richstone (1988), van der Marel et al. (1998), Joseph et al. (2001), Verolme et al. (2002), Kormendy (2004).

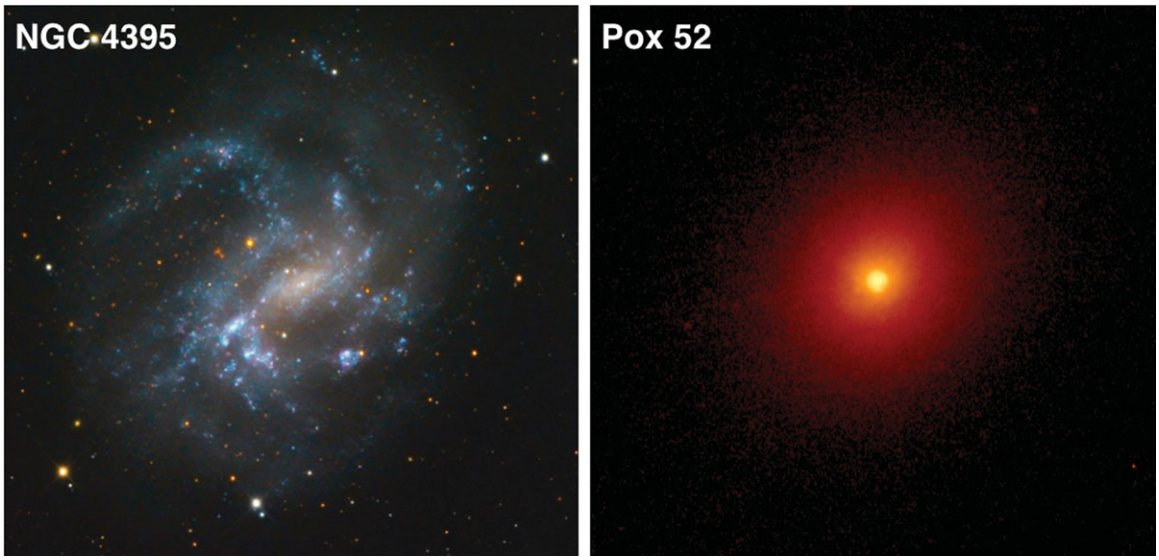

Figure 11. Prototypical examples of dwarf galaxies hosting AGN. Left: Ground-based image of NGC 4395 ($d \sim 4$ Mpc). Image courtesy of Bob Franke/Focal Pointe Observatory. Right: *HST*/ACS F814W archival image of Pox 52 using logarithmic scaling ($d \sim 90$ Mpc; also see Thornton et al. 2008).

3.2. Optically selected AGNs

The first dwarf galaxies found to host AGNs, NGC 4395 (Filippenko & Sargent 1989), and Pox 52 (Kunth et al. 1987), were discovered nearly three decades ago. NGC 4395 is a late-type dwarf spiral galaxy and Pox 52 is a dwarf elliptical (Filippenko & Ho 2003; Barth et al. 2004, see Figure 11). Both galaxies have stellar masses of $M_\star \sim 10^9 {\rm M}_\odot$ and show clear AGN signatures, including high-ionisation narrow emission lines and broad Balmer lines. NGC 4395 also exhibits a compact radio jet (Wrobel & Ho 2006) and large variability in X-rays (Vaughan et al. 2005; Moran et al. 2005). Estimates for the BH masses in these systems are on the order of a few $\times 10^5 {\rm M}_\odot$ (Peterson et al. 2005; Thornton et al. 2008), with a recent dynamical mass measurement for the BH in NGC 4395 by den Brok et al. (2015, see Table 2). For a long time, NGC 4395 and Pox 52 were the only dwarf galaxies known to host massive BHs.

Once the SDSS became available, systematic searches in the low-mass regime began. Greene & Ho (2004, 2007) conducted the first searches for *low-mass BHs* using SDSS spectroscopy (also see Dong et al. 2012, for a similar study). They searched for broad-line AGN, for which they estimated BH masses (Greene & Ho 2005), and found ∼200 objects with $M_{\rm BH} \lesssim 10^{6.5}$ M$_\odot$. These BHs, therefore, have masses comparable to or less than the BH at the centre of the Milky Way (Ghez et al. 2008). The median BH mass of the Greene & Ho (2007) sample is $\langle M_{\rm BH} \rangle \sim 1.3 \times 10^6$ M$_\odot$. Barth, Greene, & Ho (2008) conducted a complementary search for narrow-line AGN in *low-luminosity galaxies* with absolute magnitudes fainter than $M_g = -20$ mag. They present a sample of 29 objects with stellar velocity dispersions in the range $\sigma_\star \sim 40$–90 km s^{-1}. The host galaxies in the Greene & Ho (2007) and Barth et al. (2008) samples have median absolute g-band magnitudes of $\langle M_g \rangle \sim -19.3$ and $\langle M_g \rangle \sim -19.0$, respectively, and are thus sub-$L_\star$ galaxies. These samples include a few galaxies with stellar masses similar to NGC 4395 and Pox 52, however, the vast majority of the galaxies in these samples are more massive than a few $\times 10^9 {\rm M}_\odot$ and, for the most part, do not probe the dwarf galaxy regime (see Barth et al. 2008 and Figure 12 here).

Reines et al. (2013) conducted the first systematic search for active massive BHs in dwarf galaxies by analysing spectra from the SDSS, specifically targeting galaxies with

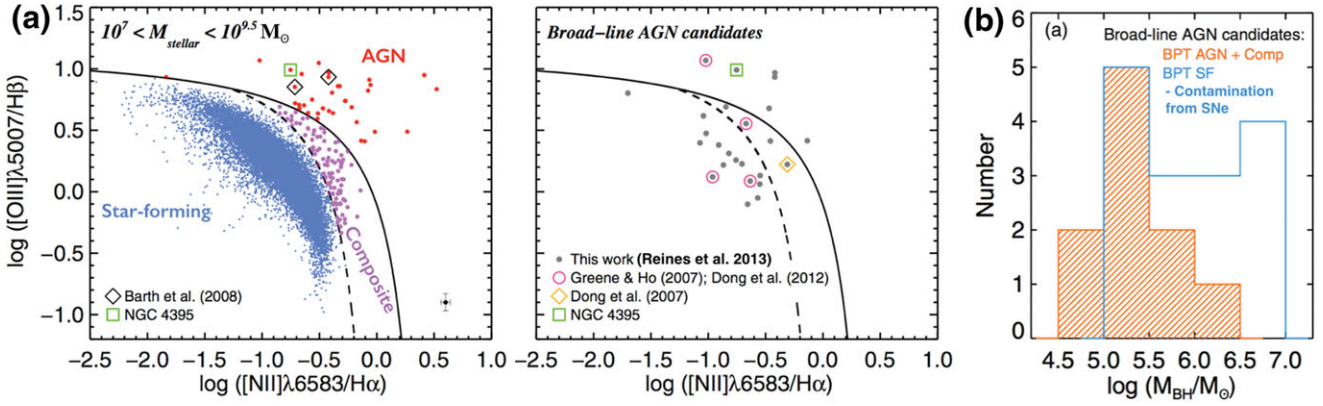

Figure 12. Optical signatures of active massive BHs in dwarf galaxies adapted from Reines et al. (2013). (a) BPT diagram for ∼25 000 dwarf emission line galaxies in the SDSS with $M_\star \lesssim 3 \times 10^9 M_\odot$ and $z < 0.055$. Thirty-five objects fall in the AGN part of the diagram (red points) and 101 objects fall in the 'composite' (AGN+SF) part of the diagram (purple points). Of these 136 dwarf galaxies with narrow-line signatures indicating an active massive BH, 10 have broad Hα emission likely signifying dense gas orbiting close to the BH. An additional 15 galaxies in the star-forming part of the BPT diagram exhibit broad Hα emission in their spectra. (b) Distribution of BH masses for the galaxies with broad Hα emission in their SDSS spectra. BH masses are calculated using equation (5) in Reines et al. (2013), which is based on the method of Greene & Ho (2005) but uses the updated radius–luminosity relationship of Bentz et al. (2013). The apparent excess at larger BH masses for the BPT star-forming objects (blue histogram) is most likely due to SNe masquerading as broad-line AGN (e.g., Baldassare et al. 2016a). For the more secure broad-line AGN candidates (BPT AGN + composites; orange histogram), the median BH mass is just $\langle M_{BH} \rangle \sim 2 \times 10^5 M_\odot$. All 10 of the broad-line AGN and composites are also detected in X-rays with *Chandra* (Baldassare et al., 2016b). © AAS. Reproduced with permission.

stellar masses $M_\star \leq 3 \times 10^9$ M$_\odot$[2] and redshifts $z \leq 0.055$. This work resulted in more than an order of magnitude increase in the number of known dwarf galaxies with massive BHs. Reines et al. (2013) present a sample of 136 dwarf galaxies with stellar masses in the range $10^{8.5} \lesssim M_\star \lesssim 10^{9.5} M_\odot$ (∼ SMC to LMC) that exhibit spectroscopic photoionisation signatures of active BHs based on standard narrow emission-line diagnostic diagrams (Kewley et al. 2006, and references therein)[3]. Of these, 35 objects fall in the AGN part of the [O III]/Hβ versus [N II]/Hα (i.e., BPT; Baldwin, Phillips, & Terlevich 1981) diagram (including NGC 4395 and two objects from the Barth et al. 2008 sample) and 101 objects fall in the 'composite' region, possibly indicating contributions from both AGN activity and star formation (Figure 12). The location of the composites in the [O III]/Hβ versus [S II]/Hα and [O III]/Hβ versus [O I]/Hα diagnostic diagrams indicates the majority of these objects have Seyfert-like line ratios and very likely do indeed host massive BHs. Broad Hα emission (FWHM ∼600–1 600 km s^{-1}) was detected in the spectra of six AGNs and four composites (including NGC 4395, two objects from the Greene & Ho 2007 sample, and the dwarf disk galaxy from Dong et al. 2007). Using standard virial techniques (see Equation 5 in Reines et al. 2013, and references therein), the range of BH masses for the 10 broad-line AGNs and composites is $M_{BH} \sim 10^5 - 10^6 M_\odot$ with a median of $\langle M_{BH} \rangle \sim 2 \times 10^5$ M$_\odot$. All 10 of these objects are detected in X-rays with *Chandra* (Baldassare et al., 2016b). The flux limit of the SDSS makes it very unlikely to detect broad-line AGNs with BH masses much less than $M_{BH} \sim 10^5 M_\odot$ at an Eddington ratio of ∼10% (Reines et al. 2013).

Follow-up observations of the Reines et al. (2013) sample has led to the discovery of a new record holder for the least-massive BH known in a galaxy nucleus. Baldassare et al. (2015) present evidence for a ∼50 000 M$_\odot$ BH at the centre of RGG 118, which has a stellar mass of $M_\star \sim 2.5 \times 10^9 M_\odot$ and was originally classified as a narrow-line composite object (Reines et al. 2013, ID 118). New Magellan spectroscopy of RGG 118, with higher sensitivity and spectral resolution than the original SDSS spectrum, displays clear broad Hα emission, which is used to estimate the BH mass. The source is also detected in X-rays with *Chandra*, providing additional support for a massive BH. The X-ray observations imply an accretion powered luminosity of $\sim 4 \times 10^{40}$ erg s^{-1} and the corresponding Eddington ratio is ∼1%, which is typical of Seyfert nuclei in more massive galaxies. Baldassare et al. (2015) measure a velocity dispersion of just ∼27 km s^{-1} and find that this object falls on the extrapolation of the $M_{BH} - \sigma_\star$ relation to the lowest masses yet (Figure 13, also see Barth, Greene, & Ho 2005 and Xiao et al. 2011).

Moran et al. (2014) present a sample of 28 AGNs in low-mass galaxies also discovered by analysing SDSS spectra and looking for AGN-like line ratios. They apply different selection criteria than Reines et al. (2013), including galaxies with stellar masses $M_\star \lesssim 10^{10}$ M$_\odot$, distances $d \leq 80$ Mpc and, for the most part, they do not include composite objects.

[2] The mass threshold for what Reines et al. (2013) considered a dwarf galaxy is equivalent to the stellar mass of the Large Magellanic Cloud (LMC; van der Marel et al. 2002), the most massive dwarf satellite galaxy of the Milky Way.

[3] Models of low-metallicity AGNs overlap with low-metallicity starbursts (Groves, Heckman, & Kauffmann 2006), and therefore the Reines et al. (2013) sample is likely highly incomplete.

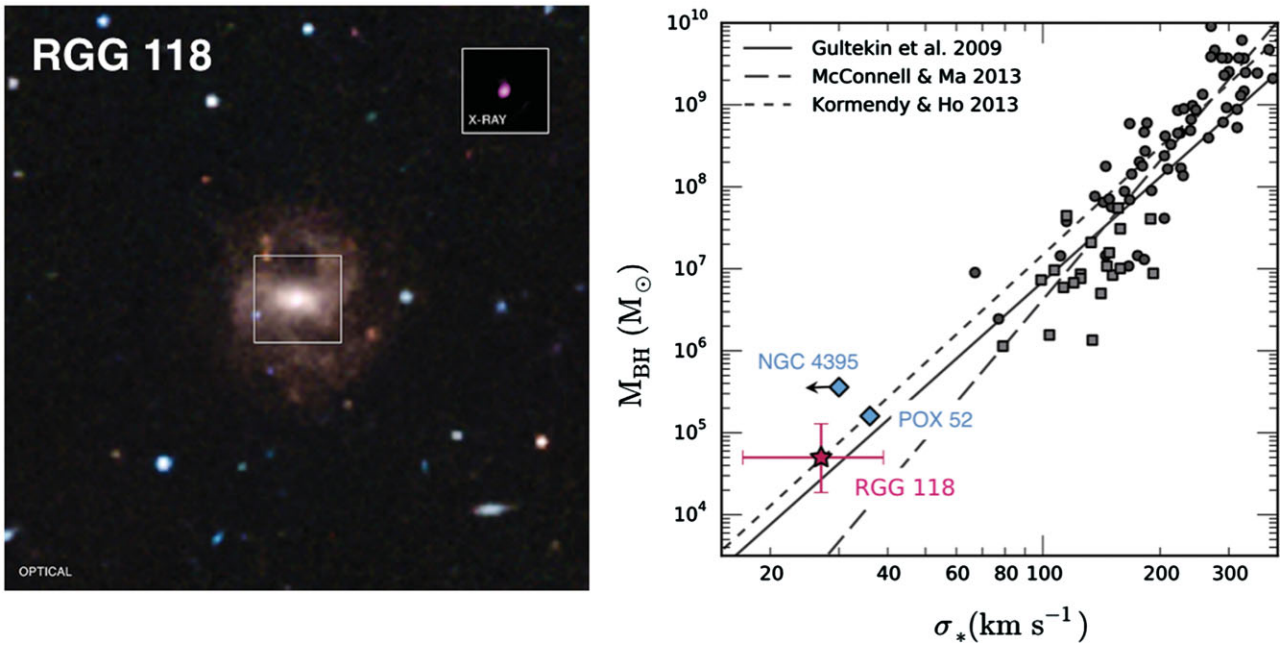

Figure 13. The dwarf galaxy RGG 118, which contains a $\sim$50 000 $M_\odot$ nuclear BH (Baldassare et al. 2015). Left: The optical image is from SDSS data and the inset shows the X-ray detection with *Chandra*. Image credit – X-ray: NASA/CXC/Univ of Michigan/V.F.Baldassare, et al; Optical: SDSS. Right: RGG 118 on the $M_{\rm BH} - \sigma_\star$ relation. From Baldassare et al. (2015). © AAS. Reproduced with permission.

An object-by-object comparison of the Moran et al. (2014) sample to the Reines et al. (2013) sample indicates that 10 objects were previously identified by Reines et al. (2013) and the remaining 18 were not in the parent sample of Reines et al. (2013), and therefore not examined in that work. The majority of these 18 objects (15/18)[4] were cut because their stellar masses are above the limit of 3×10^9 $M_\odot$ applied in Reines et al. (2013). Whilst there are systematic differences in the stellar mass estimates used by the two studies, overall, the overlap between the samples is amongst the lower mass objects in Moran et al. (2014).

Sartori et al. (2015) also searched for AGNs in dwarf galaxies using emission line measurements of SDSS galaxies provided by the OSSY catalogue (Oh et al. 2011), applying stellar mass and redshift cuts of $M_\star \lesssim 3 \times 10^9$ $M_\odot$ and $z < 0.1$. They find 48 galaxies with Seyfert-like line ratios using the BPT diagram. They also find 121 candidate AGNs using the He II λ4686/Hβ versus [N II]λ6584/Hα diagnostic diagram from Shirazi & Brinchmann (2012). All of the BPT-selected AGNs with detectable He II emission are also selected as AGNs using the Shirazi & Brinchmann (2012) criterion, but the vast majority of the He II-selected AGN candidates look like star-forming galaxies in the BPT diagram. Further investigation would be helpful to determine if the strong He II emitters are indeed AGNs.

Low-mass galaxies exhibiting broad Hα emission, yet classified as star-forming galaxies based on narrow line ratios (e.g., the BPT diagram), have also been flagged as possible AGNs in a number of studies (Greene & Ho 2007; Izotov, Thuan, & Guseva 2007; Izotov & Thuan 2008; Reines et al. 2013; Koss et al. 2014). Whilst some of these objects may indeed be bonafide AGNs, stellar processes (e.g., luminous Type II SNe, LBVs) can also account for the observed broad Hα emission in many cases. For example, follow-up spectroscopic observations of 14 broad-line objects falling in the star-forming part of the BPT diagram from Reines et al. (2013) demonstrate that the broad Hα emission either completely disappeared or was ambiguous over a time span of several years, indicating the presence of a SNe or some other transient in the original SDSS spectrum (Baldassare et al. 2016a). This is in stark contrast to the broad-line objects falling in the AGN and composite region of the BPT diagram (see Figure 14). For those with follow-up spectroscopy, Baldassare et al. (2016a) find that the broad lines persist as expected for an AGN origin. Therefore, objects exhibiting broad Balmer lines without narrow line signatures of an active BH should be treated with caution. Fast optical variability (< 1 day) in a galaxy nucleus, on the other hand, could signal an accreting low-mass BH (e.g., Morokuma et al. 2016) and help overcome the selection bias against AGNs in star-forming galaxies.

3.3. X-ray observations

AGN samples selected using optical emission lines, such as those described above, tend to be biased towards BHs radiating at moderate to high fractions of their Eddington luminosities. In contrast, X-ray observations are capable of

[4] Additionally, two objects were lost due to emission line cuts and one object does not have an accurate match in the NASA-Sloan Atlas, the catalogue used to build the parent sample in Reines et al. (2013).

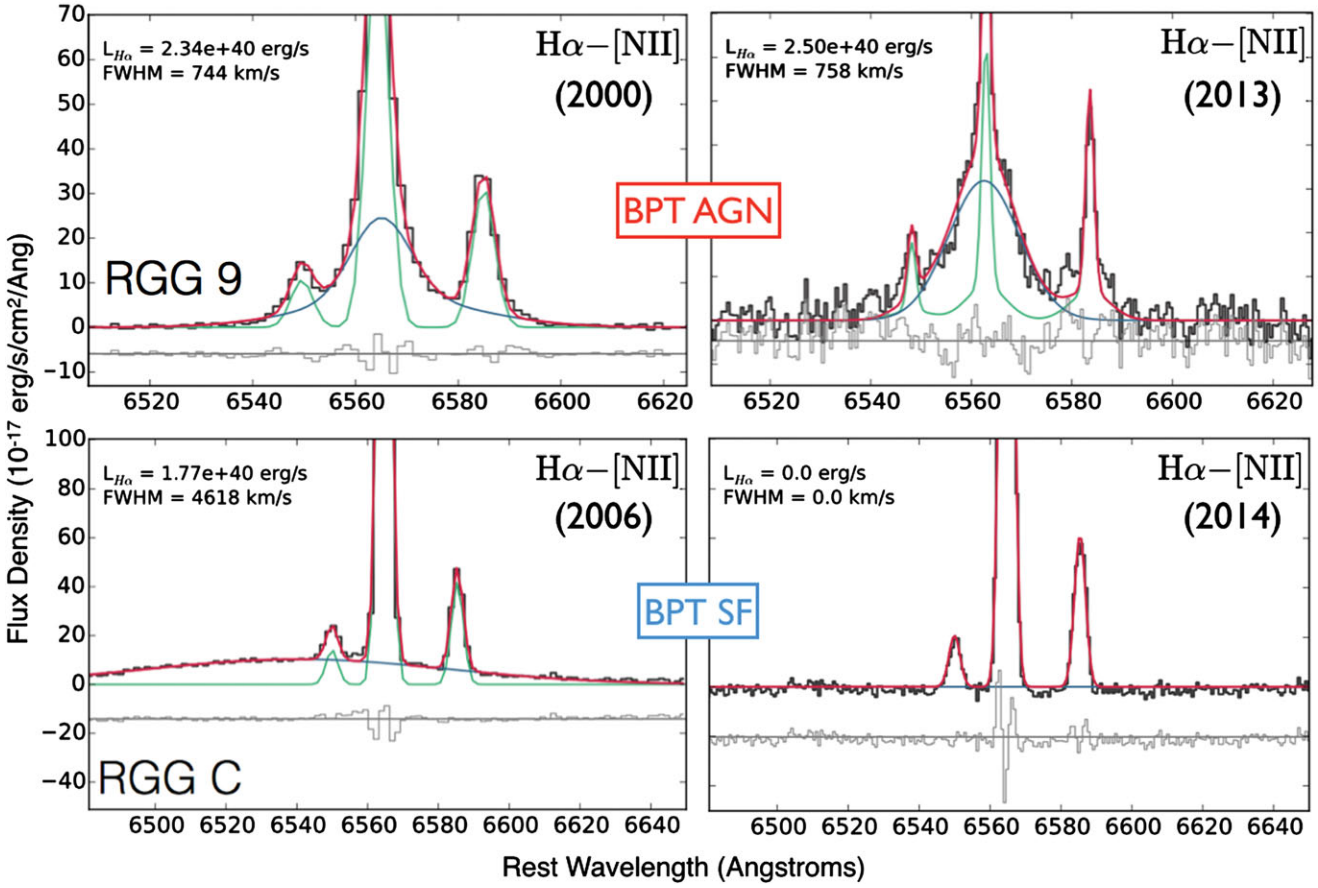

Figure 14. Multi-epoch spectroscopy of dwarf galaxies with broad Hα emission (Baldassare et al. 2016a). The top panels show two spectra of RGG 9 (a BPT AGN from Reines et al. 2013) taken more than a decade apart. The broad line is persistent, confirming an AGN origin. The bottom panels show spectra of RGG C, which has narrow emission line ratios dominated by recent star formation. The broad Hα emission has disappeared between the two epochs, indicating an SNe or other transient was responsible for the broad line originally detected in the SDSS spectrum. Adapted from Baldassare et al. (2016a).

probing BH accretion down to very low levels. For example, the AMUSE[5] surveys targeted 203 early-type galaxies within ∼30 Mpc with *Chandra* and reached a sensitivity limit of log $L_X \simeq 38.3$ erg s^{-1} (Miller et al. 2015, also see Gallo et al. 2010 and Miller et al. 2012). At such low luminosities, contamination from X-ray binaries (XRBs) becomes a concern. To minimise contamination from high-mass XRBs, the AMUSE surveys focus on early-type galaxies with low star-formation rates. Chance contamination from low-mass XRBs in the presence of a nuclear star cluster is estimated using the enclosed mass in conjunction with the shape and normalisation of the low-mass XRB luminosity function (e.g., Gallo et al. 2010). For nuclear X-ray sources very likely powered by accretion onto a massive BH in the AMUSE galaxies, the X-ray luminosities are highly sub-Eddington, typically with $L_X/L_{Edd} < 10^{-5}$.

Stellar masses of the host galaxies in the AMUSE surveys are in the range $7.7 \lesssim \log(M_\star/M_\odot) \lesssim 12$ and, whilst the vast majority of nuclear X-ray detections are in massive galaxies with $M_\star \geq 10^{10}M_\odot$, seven galaxies with $M_\star < 10^{10}M_\odot$ have detectable nuclear X-ray sources that are very likely coming from accreting massive BHs[6] (Miller et al. 2015, also see Gallo et al. 2008). Accounting for the scaling of nuclear X-ray luminosity with stellar mass, Miller et al. (2015) constrain the occupation fraction of massive BHs in early-type galaxies with $M_\star < 10^{10}M_\odot$ to be $> 20\%$.

In addition to low-mass early-type galaxies, X-ray observations have revealed small samples of massive BH candidates in late-type spiral galaxies (Ghosh et al. 2008; Desroches & Ho 2009), Lyman Break Analogs (Jia et al. 2011), dwarf irregulars (Lemons et al. 2015; Secrest et al. 2015), and blue compact dwarf galaxies (Reines et al. 2011, 2014, also see Section 3.4 below). A hard X-ray selected sample of AGNs in galaxies with $M_\star \lesssim 10^{10}M_\odot$ has recently been assembled by Chen et al. (in preparation), based on serendipitous detections by *NuSTAR*. An X-ray variability study by

[5] AGN Multiwavelength Survey of Early-Type Galaxies.

[6] An additional six galaxies with $M_\star < 10^{10}M_\odot$ have nuclear X-ray detections but LMXBs cannot be ruled out as the origin of the X-ray emission (Miller et al. 2015).

Kamizasa, Terashima, & Awaki (2012) led to the discovery of 15 candidate AGNs with $M_{\rm BH} \sim (1.1-6.6) \times 10^6 {\rm M}_\odot$, a BH mass regime similar to (or slightly larger than) the optically selected broad-line AGNs in the Greene & Ho (2007) sample. Optical spectroscopic observations by Ho & Kim (2016) detect broad Hα emission in 12 of these objects (all of those observed), confirming the sample consists of relatively low-mass BHs accreting at high Eddington ratios.

Lemons et al. (2015) leveraged the *Chandra* data archive in a systematic search for candidate BHs in dwarf galaxies with stellar masses $M_\star \lesssim 3 \times 10^9 {\rm M}_\odot$ and redshifts $z < 0.055$. They present a sample of 19 dwarf galaxies spanning a wide range in colour, specific star-formation rate and morphology, consisting of a total of 43 hard X-ray point-like sources with luminosities in the range $L_{2-10\,{\rm keV}} \sim 10^{37}$–$10^{40}$ erg s^{-1}. The majority of these sources are likely luminous stellar mass XRBs. However, some sources may be powered by more massive BHs radiating at low Eddington ratios, such as the well-studied dwarf Seyfert galaxy NGC 4395 (e.g., Filippenko & Sargent 1989; Filippenko & Ho 2003) which falls in the Lemons et al. (2015) sample. Follow-up observations, particularly at radio wavelengths (e.g., see Section 3.4 below), would help differentiate between stellar-mass and massive BHs in these dwarf galaxies.

There is a growing body of evidence for massive BHs in low-mass galaxies at moderate redshifts from deep X-ray surveys. Using the 4 Ms CDF-S survey and a stacking analysis, Xue et al. (2012) find that obscured AGNs in galaxies with stellar masses of $2 \times 10^8 \lesssim M_\star/{\rm M}_\odot \lesssim 2 \times 10^9$, blue colours, and redshifts of $1 \lesssim z \lesssim 3$ are responsible for the majority of the unresolved 6–8 keV cosmic X-ray background. Schramm et al. (2013) present a detailed study of three galaxies with $M_\star \lesssim 3 \times 10^9 {\rm M}_\odot$ at $z < 0.3$ hosting candidate AGNs that are individually detected in the CDF-S. Using the *Chandra* COSMOS-Legacy survey data, Mezcua et al. (2016) perform a stacking analysis of non-detected low-mass galaxies ($M_\star \lesssim 3 \times 10^9 {\rm M}_\odot$) in five redshift bins from $z = 0$ to $z = 1.5$. After accounting for X-ray emission from XRBs and hot ISM gas, Mezcua et al. (2016) find an excess in the stacked X-ray emission that can be attributed to accreting massive BHs. Using deep archival *Chandra* observations overlapping with the NEWFIRM Medium-Band Survey, Pardo et al. (2016) identify 10 dwarf galaxies at redshifts $0.1 \lesssim z \lesssim 0.6$ (from DEEP2 spectroscopy) exhibiting X-ray emission consistent with AGN activity (see Figure 15).

At higher redshifts, $z \gtrsim$5–6, few if any AGNs have been detected in galaxies with stellar masses $M_\star \sim 10^9 {\rm M}_\odot$, either through direct X-ray detections (Fiore et al. 2012a; Giallongo et al. 2015; Weigel et al. 2015; Cappelluti et al. 2016) or stacking of Lyman Break Galaxies (LBGs) (Willott 2011; Cowie et al. 2012; Treister et al. 2013; Vito et al. 2016). Extrapolating local BH mass to bulge mass relations defined by early-type galaxies (e.g., Marconi & Hunt 2003; Häring & Rix 2004; Kormendy & Ho 2013) would suggest a higher detection rate. However, Volonteri & Reines (2016) demonstrate that the non-detections can be accounted for by instead extrapolating the local BH to total stellar mass relation of Reines & Volonteri (2015), which has a significantly lower normalisation and is defined by moderate-luminosity AGNs predominantly in lower mass later-type galaxies.

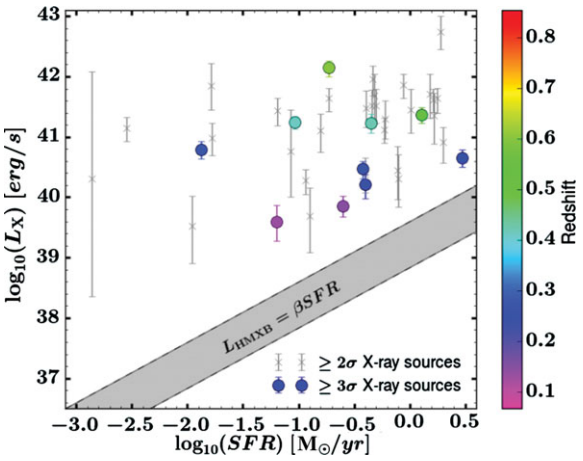

Figure 15. X-ray luminosity versus star formation rate for the dwarf galaxies identified by Pardo et al. (2016). The X-ray luminosities are well above the expected contribution from high-mass X-ray binaries and are consistent with an AGN origin. From Pardo et al. (2016). © AAS. Reproduced with permission.

3.4. Combined radio + X-ray searches

The combination of sensitive, high-resolution radio, and X-ray observations offer a promising path forward in the search for massive BHs in dwarf galaxies. These observations can detect weakly accreting BHs, as well as those living in dwarf galaxies with ongoing star formation that can hide BH accretion signatures at optical wavelengths. Moreover, radio observations can help break the degeneracy at X-ray luminosities that are consistent with either luminous stellar-mass XRBs or more massive BHs radiating at low Eddington ratios (e.g., Merloni, Heinz, & di Matteo 2003; Falcke, Körding, & Markoff 2004; Plotkin et al. 2012). For a given X-ray luminosity, massive BHs are significantly more luminous in the radio than stellar-mass BHs. Unfortunately, existing radio and X-ray surveys are either too shallow and/or lack sufficient angular resolution to reliably identify AGNs in dwarf galaxies. There are other potential sources of compact radio and X-ray emission, particularly in star-forming dwarf galaxies (e.g., H II regions, supernovae, supernova remnants, XRBs, hot X-ray gas from star formation), and therefore a careful multiwavelength approach must be employed that is currently only possible with dedicated observations.

Reines et al. (2011) present evidence for a massive BH in the dwarf starburst galaxy Henize 2–10. Optical spectroscopy of Henize 2–10 is dominated by star formation, yet VLA and *Chandra* observations reveal a compact source of radio and X-ray emission[7] strongly suggesting a massive BH at the

[7] For additional studies of the radio and X-ray emission from Henize 2–10, see Kobulnicky & Johnson (1999), Johnson & Kobulnicky (2003), Kobulnicky & Martin (2010), and Whalen et al. (2015).

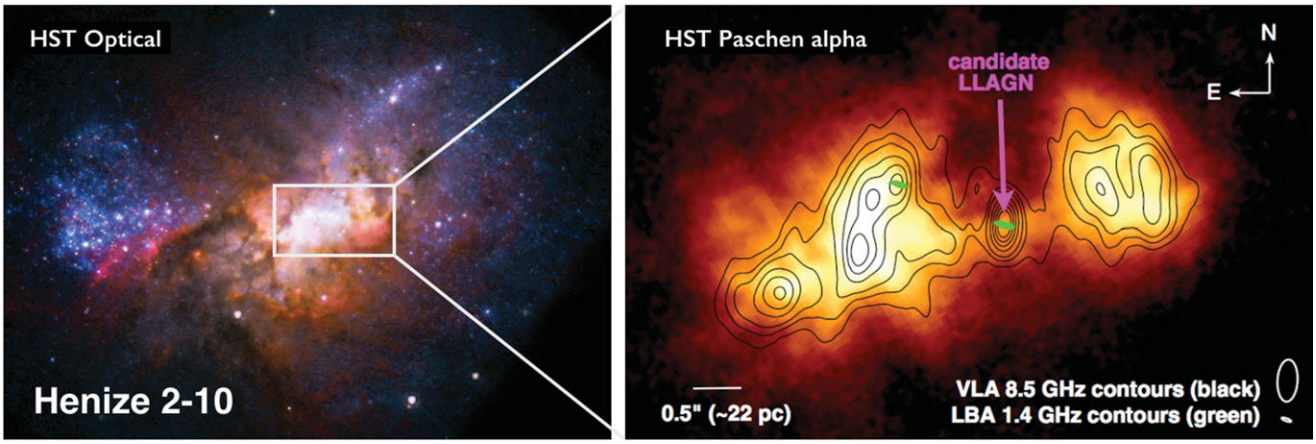

Figure 16. Left: *HST* optical image of Henize 2–10, a dwarf starburst galaxy with a massive BH (Reines et al. 2011). Right: *HST* narrow-band Paα image of the central few hundred parsecs of the galaxy showing ionised gas emission. Black contours indicate radio emission detected with the VLA and green contours show the VLBI detection from Reines & Deller (2012). Reines et al. (2016) present a study of the X-ray emission from the massive BH using deep *Chandra* observations. © AAS. Reproduced with permission.

centre of the galaxy (see Reines et al. 2016 for new, deep *Chandra* observations of Henize 2–10). Furthermore, follow-up Very Long Baseline Interferometry observations by Reines & Deller (2012) detect a parsec-scale, non-thermal radio core at the precise position of the central source, providing additional support for a massive BH. A comparison with *HST* narrow-band Hα and Paα imaging demonstrates that the BH lies at the centre of a $\sim$250 pc-long ionised gas structure with a morphology suggestive of bipolar flow (Figure 16; also see Figure 2 in Reines et al. 2011). No star cluster is detected at the location of the BH in Henize 2–10 (Reines et al. 2011); however, several young massive ($\sim 10^5 - 10^6 M_\odot$) star clusters reside within the central region of the galaxy (e.g., Johnson et al. 2000; Chandar et al. 2003; Nguyen et al. 2014). The dynamical friction timescales for the most massive clusters to reach the centre of the galaxy are only a few hundred Myr, suggesting a nuclear star cluster will form around the pre-existing BH in a relatively short time (Nguyen et al. 2014). *N*-body simulations modelling the future evolution of the central clusters and the BH in Henize 2–10 come to the same conclusion (Arca-Sedda et al. 2015). Estimates for the total stellar mass of Henize 2–10 are in the range $M_\star \sim 10^9 - 10^{10} M_\odot$ (Reines et al. 2011; Kormendy & Ho 2013; Nguyen et al. 2014), a mass regime in which the coexistence of nuclear star clusters and massive BHs is very common (Seth et al. 2008).

A continued search for massive BHs in dwarf star-forming galaxies using the combination of high-resolution radio and X-ray observations has led to the discovery of a candidate AGN in Mrk 709 (Reines et al. 2014). Mrk 709 is a low-metallicity (Masegosa, Moles, & Campos-Aguilar 1994) blue compact dwarf (Gil de Paz, Madore, & Pevunova 2003) that appears to be a pair of interacting galaxies with stellar masses of $M_\star \sim 1.1 \times 10^9 M_\odot$ (Mrk 709 N) and $M_\star \sim 2.5 \times 10^9 M_\odot$ (Mrk 709 S) (Reines et al. 2014). VLA and *Chandra* observations reveal spatially coincident (within the astrometric uncertainties) radio and hard X-ray point sources at the centre of the southern galaxy, Mrk 709 S, with luminosities suggesting the presence of an accreting massive BH. With a metallicity of only $\sim$10% of the solar value, Mrk 709 is amongst the most metal-poor galaxies with evidence for a massive BH. Given the low metallicity, copious star formation, as well as the interaction, Mrk 709 may be a good local analogue of higher redshift systems of similar mass.

3.5. Mid-infrared searches

Observations at mid-infrared wavelengths, for example with *Spitzer* and the *Wide-field Infrared Survey Explorer (WISE)*, have proved useful for finding obscured and unobscured luminous AGNs out to high redshifts. In recent years, a number of studies have extrapolated *WISE* AGN diagnostics (Jarrett et al. 2011; Stern et al. 2012) to low-bulge and low-mass galaxies (Satyapal et al. 2014; Marleau et al. 2014; Sartori et al. 2015; Hainline et al. 2016).

The mid-infrared selection technique relies on distinguishing the broadband colours of dust heated to high temperatures by AGNs (roughly a power law spectrum) from other sources of mid-infrared emission. The mid-infrared colours of luminous AGNs are clearly distinct from stars and normal galaxies that have blackbody spectra at long wavelengths. However, mid-infrared colour cuts for AGNs can overlap with the colours of star-forming galaxies, which can also exhibit red *WISE* colours from hot dust emission. This is particularly consequential for dwarf star-forming galaxies that can have integrated mid-infrared photometry completely dominated by a young starburst (e.g., Griffith et al. 2011; Izotov et al. 2011, 2014). Indeed, Hainline et al. (2016) clearly demonstrate that star-forming dwarf galaxies, particularly those with

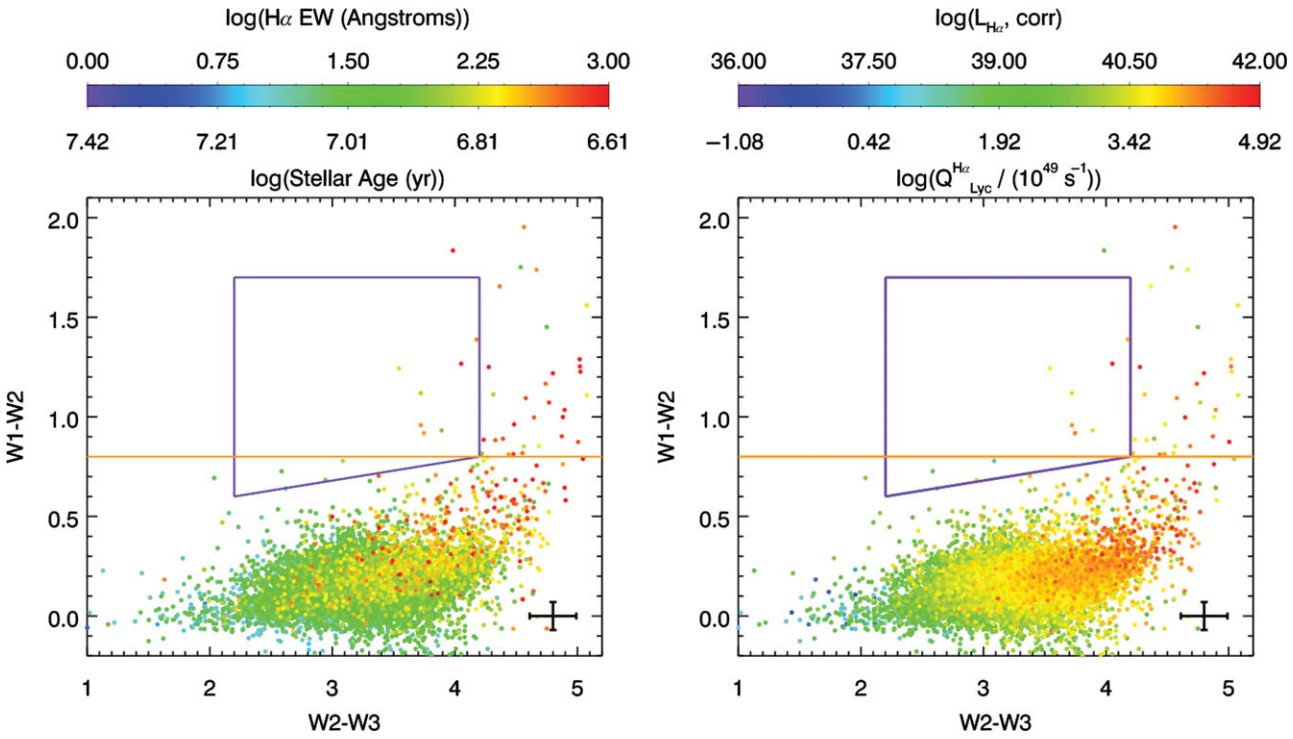

Figure 17. *WISE* mid-infrared colour–colour diagram for optically selected star-forming dwarf galaxies ($M_\star \leq 3 \times 10^9 M_\odot$) within $z \leq 0.055$. Left: Points are colour-coded by the equivalent width of the Hα emission line, which is anticorrelated with stellar age (Leitherer et al. 1999). Right: Points are colour-coded by Hα luminosity, which is correlated with ionising flux and star-formation rate (e.g., Condon 1992; Kennicutt & Evans 2012). The dwarf galaxies with the reddest *WISE* colours are optically blue and compact, with young stellar populations and high specific star-formation rates (Hainline et al. 2016). The star-forming sequence wraps around and largely avoids the Jarrett et al. (2011) AGN selection box shown in blue. However, the star-forming dwarf galaxies with the reddest *WISE* colours satisfy the canonical (luminous) AGN selection criterion of $W1 - W2 \geq 0.8$ from Stern et al. (2012, orange line). Therefore, caution should be exercised when attempting to select AGNs in dwarf galaxies using infrared colours, as star-forming dwarfs can heat dust in such a way that mimics luminous AGNs. From Hainline et al. (2016). © AAS. Reproduced with permission.

very young stellar populations ($t \lesssim 5$ Myr) and high specific SFRs, can have mid-infrared colours overlapping those of *WISE*-selected AGNs (Figure 17).

Given the confusion between dwarf starburst galaxies and luminous AGNs in mid-infrared colour space, red *WISE* colours alone should not necessarily be taken as evidence for AGNs in low-mass galaxies. Contamination from star-forming galaxies may also help explain one particularly puzzling result first found by Satyapal et al. (2014), and also seen to some extent by Marleau et al. (2014) and Sartori et al. (2015). All of these studies claim the mid-infrared AGN fraction actually *increases* at very low-galaxy masses ($M_\star \sim 10^6$–$10^8 M_\odot$) relative to higher mass galaxies, in contrast to what is found in optical studies. This is surprising given that the BH occupation fraction is generally expected to drop with decreasing stellar mass. Furthermore, at the time of writing, no galaxy with a stellar mass $M_\star \lesssim 10^8 M_\odot$ has evidence for a massive BH at either optical or X-ray wavelengths.

3.6. Future outlook

In recent years, we have made significant progress finding and characterising AGNs in dwarf galaxies. To maximise the utility of these types of systems in constraining seed-formation mechanisms, we now need a more complete census of massive BHs in $z \sim 0$ low-mass galaxies and to accurately measure BH masses and host galaxy properties (see Figure 1 and Section 1).

In the near term, it would be useful to obtain larger samples of broad-line AGNs in dwarf galaxies with very low-BH masses and continue to populate the low-mass end of the $M_{\rm BH} - \sigma_\star$ relation (e.g., Baldassare et al. 2015, 2016a; Bentz et al. 2016), a key discriminant between BH seed-formation mechanisms. We can also use observations with the VLA to search for compact sources of radio emission at the centres of dwarf galaxies that could indicate low-level nuclear activity (e.g., Reines et al. 2011). The exquisite sensitivity provided by the upgrade to the VLA now makes large surveys of such objects feasible. X-ray observations with *Chandra* could provide the necessary follow-up data to confirm BH candidates. Such an approach has the potential to more tightly constrain the BH occupation fraction at low mass (another primary diagnostic of seed formation) than is currently possible with optically selected spectroscopic AGN samples that are biased towards higher Eddington ratios and host galaxies with relatively low levels of star formation (e.g., Reines et al. 2013). Optical variability studies using large imaging surveys

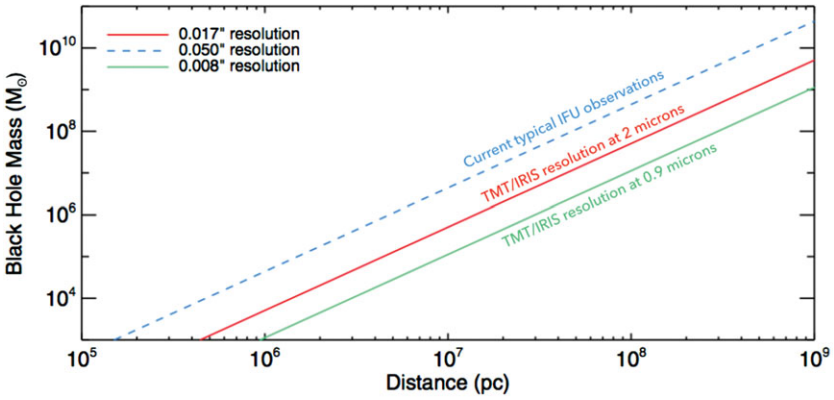

Figure 18. The spatial resolution of 30-m class telescopes will dramatically increase the accessible volume for dynamical BH searches, enabling the detection of low-mass BHs ($M_{\rm BH} \sim 10^5 {\rm M}_\odot$) in dwarf galaxies well beyond the Local Group. Adapted from Do et al. (2014). © AAS. Reproduced with permission.

could also push to low-accretion rates and help overcome the bias against finding active massive BHs in star-forming dwarf galaxies.

With LSST on the horizon, tidal disruptions of stars may prove useful for detecting otherwise quiescent BHs in dwarf galaxies (e.g., MacLeod et al. 2016; also see Miller & Gültekin 2011, Yoon et al. 2015, Maksym, Lin, & Irwin 2014a, Maksym et al. 2014b, and Donato et al. 2014 for current candidates in the low-mass regime). Further down the road, the next generation of large (∼30–40 m) ground-based telescopes will revolutionise our understanding of BH demographics in local dwarf galaxies. Dynamical searches, for example with the Thirty-Meter Telescope (TMT), the Giant Magellan Telescope (GMT), and the E-ELT, could provide robust masses (or upper limits) on quiescent BHs in dwarf galaxies that are currently out of reach (e.g., see Figure 18), and thereby reliably determine the BH occupation fraction (rather than the *active* fraction) at low masses.

4 CONCLUSIONS

Efforts to observationally constrain the birth and growth of massive BHs have advanced considerably in recent years. There are ever growing samples of high-redshift quasars with giant BHs, and smaller and smaller BHs are being discovered in nearby dwarf galaxies. What are these observations telling us about the formation of the first BH seeds?

There are hints from the quasar population that massive seeds ($M_{\rm seed} \sim 10^5 {\rm M}_\odot$) may be preferred over lighter stellar-mass seeds ($M_{\rm seed} \sim 10^2 {\rm M}_\odot$). For example, Natarajan & Volonteri (2012) compare the BH mass function of luminous broad-line quasars in the SDSS from $1 < z < 4.5$ (Kelly et al. 2010) with merger-driven BH growth models. They find that models with low-mass seeds underproduce the massive end of the BH mass function from intermediate to high redshifts, even when the BHs are accreting at the Eddington rate at all times. Natarajan & Volonteri (2012) conclude that stellar-mass seeds would have had to undergone extreme growth conditions (e.g., super-Eddington accretion; also see Madau et al. 2014) or BH seeds were significantly more massive.

We also have some clues from $z \sim 0$ dwarf galaxies. The existence of BHs with masses overlapping those predicted by some seed-formation models ($M_{\rm BH} \sim 10^5 {\rm M}_\odot$) demonstrates that BHs do indeed extend to such low masses. It remains to be seen, however, how low they go. Detecting even smaller BHs and measuring their masses is difficult with current observational capabilities. The current record-holder for the least-massive nuclear BH known is $M_{\rm BH} \sim 5 \times 10^4 {\rm M}_\odot$ (Baldassare et al. 2015) in the dwarf galaxy RGG 118 (Reines et al. 2013). In addition to pushing to lower BH masses, we would like to compare observational results to predictions for the BH occupation fraction and scaling relations at low mass for various seed models (e.g., Figure 1). Spectroscopic selection of AGNs in dwarfs have produced the largest samples, but they only place a lower limit on the BH occupation fraction. Moreover, the selection effects are severe and challenging to quantify. Currently, the best constraints on the local BH occupation fraction in low-mass galaxies come from sensitive X-ray observations, but the implications for BH seeding are inconclusive (Miller et al. 2015). We are beginning to populate the very low mass end of the $M_{\rm BH} - \sigma_\star$ relation (e.g., Baldassare et al. 2016a), but there are not yet enough objects to reliably distinguish between models of BH seed formation using this diagnostic. It is interesting to note, however, that the simulated BHs with seed masses of $M_{\rm BH} \sim 10^3 {\rm M}_\odot$ from Habouzit et al. (2016) eventually grow and connect to the low-redshift sample of broad-line AGNs from Reines & Volonteri (2015) in the $M_{\rm BH} - M_\star$ plane.

The dearth of detectable X-ray emitting AGNs in high-redshift ($z > 6$) Lyman Break Galaxies (LBGs) provides additional constraints on the early growth of massive BHs (e.g., Cowie et al. 2012; Fiore, Puccetti, & Mathur 2012b; Treister et al. 2013). LBGs with typical stellar masses of $M_\star \sim 10^9 {\rm M}_\odot$ were massive galaxies at $z \sim 6$, and it is expected that they would have been seeded with a BH by that time (Volonteri 2010). Volonteri & Reines (2016) demonstrate that the

current non-detections of moderate-luminosity AGNs from stacking high-redshift LBGs can be explained if the BHs in these galaxies have masses on the order of $M_{\rm BH} \sim 10^5 {\rm M}_{\odot}$, as for local AGN host galaxies of similar mass (Reines & Volonteri 2015). If this is indeed the case, the implication is that BH seeds must be lower than or comparable to this mass.

The deepest search for X-ray emission in high-redshift galaxies using the 7 Ms CDF-S observations suggests that the faint end of the AGN luminosity function at high redshift has a fairly flat slope, which may favor heavy ($M_{\rm BH} \sim 10^4 - 10^5 {\rm M}_{\odot}$) BH seeds (Vito et al. 2016). The lack of bonafide X-ray selected AGN at $z > 6$ may be due to insufficient coverage of the area versus flux plane of current X-ray surveys and the lack of sensitive spectroscopy in the near-infrared. Future dedicated *Chandra* surveys coupled with deep near-infrared *JWST* and sub-millimetre ALMA spectroscopy will pave the way for the next generation of X-ray observatories (*ATHENA* and the X-ray Surveyor) and extremely large ground-based telescopes (E-ELT, TMT, GMT).

Although we do not yet have a definitive answer regarding the origin of the first BH seeds, there are many reasons to be optimistic about the future (e.g., see Sections 2.3 and 3.6). The theoretical and observational groundwork has already been laid. We are now in a position to capitalise on new and upcoming instruments, telescopes and large surveys, and compare the observational results to ever more sophisticated models.

ACKNOWLEDGEMENTS

We thank Rosa Valiante, Rafaella Schneider, and Marta Volonteri for organising the EWASS symposium 'Understanding the growth of the first supermassive black holes' and for the opportunity to write this review. We also thank Marta Volonteri, Jenny Greene, and the anonymous referee for providing useful comments that improved the manuscript. AER is grateful for the support of NASA through Hubble Fellowship grant HST-HF2-51347.001-A awarded by the Space Telescope Science Institute, which is operated by the Association of Universities for Research in Astronomy, Inc., for NASA, under contract NAS 5-26555. AC acknowledges the longstanding collaborators of the Bologna high energy astrophysics group: Marcella Brusa, Nico Cappelluti, Francesca Civano, Roberto Gilli, Giorgio Lanzuisi, Elisabeta Lusso, Stefano Marchesi, Marco Mignoli, Cristian Vignali, Fabio Vito for very useful discussions. James Aird is warmly thanked for providing data for Figure 7 and for his contribution to conceive and develop the Athena surveys strategy. Financial contribution from the PRIN–INAF–2014, the ASI-INAF 2014-045-R.0 grants is acknowledged.

REFERENCES

Agarwal, B., et al. 2016, MNRAS, 460, 4003
Aird, J., et al. 2015, MNRAS, 451, 1892
Aird, J., et al. 2013, e-prints (arXiv:1306.2325)
Alexander, T., & Natarajan, P. 2014, Science, 345, 1330
Arca-Sedda, M., Capuzzo-Dolcetta, R., Antonini, F., & Seth, A. 2015, ApJ, 806, 220
Baldassare, V. F., Reines, A. E., Gallo, E., & Greene, J. E. 2016b, e-prints (arXiv:1609.07148)
Bañados, E., et al. 2014, AJ, 148, 14
Bañados, E., et al. 2016, e-prints (arXiv:1608.03279)
Baldassare, V. F., Reines, A. E., Gallo, E., & Greene, J. E. 2015, ApJ, 809, L14
Baldassare, V. F., et al. 2016a, ApJ, 829, 57
Baldassare, V. F., Reines, A. E., Gallo, E., & Greene, J. E. 2016b, e-prints (arXiv:1609.07148)
Baldwin, J. A., Phillips, M. M., & Terlevich, R. 1981, PASP, 93, 5
Barth, A. J., Greene, J. E., & Ho, L. C. 2005, ApJ, 619, L151
Barth, A. J., Greene, J. E., & Ho, L. C. 2008, AJ, 136, 1179
Barth, A. J., Ho, L. C., Rutledge, R. E., & Sargent, W. L. W. 2004, ApJ, 607, 90
Barth, A. J., Strigari, L. E., Bentz, M. C., Greene, J. E., & Ho, L. C. 2009, ApJ, 690, 1031
Begelman, M. C., Volonteri, M., & Rees, M. J. 2006, MNRAS, 370, 289
Bellovary, J., et al. 2011, ApJ, 742, 13
Bentz, M. C., et al. 2016, e-prints (arXiv:1608.03893)
Bentz, M. C., et al. 2013, ApJ, 767, 149
Bowler, R. A. A., et al. 2016, e-prints (arXiv:1609.00727)
Brusa, M., et al. 2009, ApJ, 693, 8
Buchner, J., et al. 2015, ApJ, 802, 89
Calura, F., et al. 2014, MNRAS, 438, 2765
Cappelluti, N., et al. 2016, ApJ, 823, 95
Carnall, A. C., et al. 2015, MNRAS, 451, L16
Chandar, R., Leitherer, C., Tremonti, C., & Calzetti, D. 2003, ApJ, 586, 939
Choi, J.-H., Shlosman, I., & Begelman, M. C. 2015, MNRAS, 450, 4411
Civano, F., et al. 2011, ApJ, 741, 91
Civano, F., et al. 2016, ApJ, 819, 62
Condon, J. J. 1992, ARA&A, 30, 575
Cowie, L. L., Barger, A. J., & Hasinger, G. 2012, ApJ, 748, 50
Davies, M. B., Miller, M. C., & Bellovary, J. M. 2011, ApJ, 740, L42
den Brok, M., et al. 2015, ApJ, 809, 101
De Rosa, G., Decarli, R., Walter, F., et al. 2011, ApJ, 739, 56
Desroches, L.-B., & Ho, L. C. 2009, ApJ, 690, 267
Devecchi, B., & Volonteri, M. 2009, ApJ, 694, 302
Do, T., et al. 2014, AJ, 147, 93
Donato, D., et al. 2014, ApJ, 781, 59
Dong, X., et al. 2007, ApJ, 657, 700
Dong, X.-B., et al. 2012, ApJ, 755, 167
Dressler, A., & Richstone, D. O. 1988, ApJ, 324, 701
Edge, A., et al. 2013, Msngr, 154, 32
Falcke, H., Körding, E., & Markoff, S. 2004, A&A, 414, 895
Fan, X. 2012, RAA, 12, 865
Fan, X., Strauss, M. A., Schneider, D. P., et al. 2003, AJ, 125, 1649
Fan, X., Hennawi, J. F., Richards, G. T., et al. 2004, AJ, 128, 515
Fan, X., et al. 2001, AJ, 122, 2833
Fan, X., Strauss, M. A., Richards, G. T., et al. 2006, AJ, 131, 1203
Filippenko, A. V., & Ho, L. C. 2003, ApJ, 588, L13
Filippenko, A. V., & Sargent, W. L. W. 1989, ApJ, 342, L11
Fiore, F., et al. 2012a, A&A, 537, A16
Fiore, F., Puccetti, S., & Mathur, S. 2012b, AdAst, 2012, 271502
Gallo, E., et al. 2008, ApJ, 680, 154
Gallo, E., et al. 2010, ApJ, 714, 25
Gebhardt, K., et al. 2001, AJ, 122, 2469
Georgakakis, A., et al. 2015, MNRAS, 453, 1946

Ghez, A. M., et al. 2008, ApJ, 689, 1044
Ghosh, H., Mathur, S., Fiore, F., & Ferrarese, L. 2008, ApJ, 687, 216
Giallongo, E., et al. 2015, A&A, 578, A83
Gil de Paz, A., Madore, B. F., & Pevunova, O. 2003, ApJS, 147, 29
Glikman, E., et al. 2011, ApJ, 728, L26
Green, P. J., et al. 2009, ApJ, 690, 644
Greene, J. E. 2012, NatCo, 3, 1304
Greene, J. E., & Ho, L. C. 2004, ApJ, 610, 722
Greene, J. E., & Ho, L. C. 2005, ApJ, 630, 122
Greene, J. E., & Ho, L. C. 2007, ApJ, 670, 92
Griffith, R. L., et al. 2011, ApJ, 736, L22
Groves, B. A., Heckman, T. M., & Kauffmann, G. 2006, MNRAS, 371, 1559
Habouzit, M., Volonteri, M., & Dubois, Y. 2016, e-prints (arXiv:1605.09394)
Haiman, Z., & Loeb, A. 2001, ApJ, 552, 459
Hainline, K. N., Reines, A. E., Greene, J. E., & Stern, D. 2016, ApJ, submitted (arXiv: 1609.06721)
Häring, N., & Rix, H.-W. 2004, ApJL, 604, L89
Hartwig, T., et al. 2016, MNRAS, 462, 2184
Hirschmann, M., Somerville, R. S., Naab, T., & Burkert, A. 2012, MNRAS, 426, 237
Ho, L., & Kim, M. 2016, ApJ, 821, 48
Ikeda, H., et al. 2011, ApJ, 728, L25
Izotov, Y. I., Guseva, N. G., Fricke, K. J., & Henkel, C. 2011, A&A, 536, L7
Izotov, Y. I., Guseva, N. G., Fricke, K. J., & Henkel, C. 2014, A&A, 561, A33
Izotov, Y. I., & Thuan, T. X. 2008, ApJ, 687, 133
Izotov, Y. I., Thuan, T. X., & Guseva, N. G. 2007, ApJ, 671, 1297
Jardel, J. R., & Gebhardt, K. 2012, ApJ, 746, 89
Jarrett, T. H., et al. 2011, ApJ, 735, 112
Jia, J., et al. 2011, ApJ, 731, 55
Jiang, L., et al. 2008, AJ, 135, 1057
Jiang, L., et al. 2009, AJ, 138, 305
Jiang, L., et al. 2010, Nature, 464, 380
Johnson, J. L., & Haardt, F. 2016, PASA, 33, 7
Johnson, K. E., & Kobulnicky, H. A. 2003, ApJ, 597, 923
Johnson, K. E., Leitherer, C., Vacca, W. D., & Conti, P. S. 2000, AJ, 120, 1273
Joseph, C. L., et al. 2001, ApJ, 550, 668
Kaiser, N., et al. 2002, in Proc. SPIE, Vol. 4836, Survey and Other Telescope Technologies and Discoveries, eds. J. A. Tyson & S. Wolff (Bellingham: SPIE), 154
Kalfountzou, E., Civano, F., Elvis, M., Trichas, M., & Green, P. 2014, MNRAS, 445, 1430
Kamizasa, N., Terashima, Y., & Awaki, H. 2012, ApJ, 751, 39
Kashikawa, N., et al. 2015, ApJ, 798, 28
Kelly, B. C., et al. 2010, ApJ, 719, 1315
Kennicutt, R. C., & Evans, N. J. 2012, ARA&A, 50, 531
Kewley, L. J., Groves, B., Kauffmann, G., & Heckman, T. 2006, MNRAS, 372, 961
Kim, M., et al. 2007, ApJ, 659, 29
Kobulnicky, H. A., & Johnson, K. E. 1999, ApJ, 527, 154
Kobulnicky, H. A., & Martin, C. L. 2010, ApJ, 718, 724
Kormendy, J. 2004, in Coevolution of Black Holes and Galaxies, ed. L. C. Ho (Cambridge: Cambridge University Press), 169
Kormendy, J., & Ho, L. C. 2013, ARAA, 51, 511
Koss, M., et al. 2014, MNRAS, 445, 515
Kunth, D., Sargent, W. L. W., & Bothun, G. D. 1987, AJ, 93, 29
LaMassa, S. M., et al. 2016, ApJ, 817, 172
Latif, M. A., & Ferrara, A. 2016, e-prints (arXiv:1605.07391)
Lawrence, A., et al. 2007, MNRAS, 379, 1599
Leitherer, C., et al. 1999, ApJS, 123, 3
Lemons, S. M., Reines, A. E., Plotkin, R. M., Gallo, E., & Greene, J. E. 2015, ApJ, 805, 12
Lodato, G., & Natarajan, P. 2006, MNRAS, 371, 1813
Loeb, A., & Rasio, F. A. 1994, ApJ, 432, 52
Lora, V., Sánchez-Salcedo, F. J., Raga, A. C., & Esquivel, A. 2009, ApJ, 699, L113
Lupi, A., Colpi, M., Devecchi, B., Galanti, G., & Volonteri, M. 2014, MNRAS, 442, 3616
Lusso, E., et al. 2011, A&A, 534, A110
MacLeod, M., Guillochon, J., Ramirez-Ruiz, E., Kasen, D., & Rosswog, S. 2016, ApJ, 819, 3
Madau, P., Haardt, F., & Dotti, M. 2014, ApJ, 784, L38
Madau, P., & Rees, M. J. 2001, ApJ, 551, L27
Maksym, W. P., Lin, D., & Irwin, J. A. 2014a, ApJ, 792, L29
Maksym, W. P., et al. 2014b, MNRAS, 444, 866
Marchesi, S., et al. 2016, ApJ, 817, 34
Marchesi, S., et al. 2016, ApJ, 827, 150
Marconi, A., & Hunt, L. K. 2003, ApJ, 589, L21
Marleau, F. R., Clancy, D., Bianconi, M., & Habas, R. 2014, e-prints (arXiv:1411.3844)
Masegosa, J., Moles, M., & Campos-Aguilar, A. 1994, ApJ, 420, 576
Matsuoka, Y., et al. 2016, ApJ, 828, 26
McGreer, I. D., et al. 2013, ApJ, 768, 105
Merloni, A., Heinz, S., & di Matteo, T., 2003, MNRAS, 345, 1057
Merloni, A., et al. 2012, e-prints (arXiv:1209.3114)
Mezcua, M., Civano, F., Fabbiano, G., Miyaji, T., & Marchesi, S. 2016, ApJ, 817, 20
Miller, B., Gallo, E., Treu, T., & Woo, J.-H. 2012, ApJ, 747, 57
Miller, B. P., et al. 2015, ApJ, 799, 98
Miller, J. M., & Gültekin, K. 2011, ApJ, 738, L13
Miyaji, T., et al. 2015, ApJ, 804, 104
Moran, E. C., et al. 2005, AJ, 129, 2108
Moran, E. C., Shahinyan, K., Sugarman, H. R., Vélez, D. O., & Eracleous, M. 2014, AJ, 148, 136
Morokuma, T., et al. 2016, PASJ, 68, 40
Morselli, L., et al. 2014, A&A, 568, A1
Mortlock, D. J., et al. 2009, A&A, 505, 97
Mortlock, D. J., et al. 2011, Nature, 474, 616
Nandra, K., et al. 2013, e-prints (arXiv:1306.2307)
Natarajan, P., & Volonteri, M. 2012, MNRAS, 422, 2051
Neumayer, N., & Walcher, C. J. 2012, Advances in Astronomy, 2012, 709038
Nguyen, D. D., et al. 2014, ApJ, 794, 34
Oh, K., Sarzi, M., Schawinski, K., & Yi, S. K. 2011, ApJS, 195, 13
Pacucci, F., et al. 2016, MNRAS, 459, 1432
Pallottini, A., et al. 2015, MNRAS, 453, 2465
Pardo, K., et al. 2016, e-prints (arXiv:1603.01622)
Pentericci, L., et al. 2016, ApJL, 829, L11
Peterson, B. M., et al. 2005, ApJ, 632, 799
Pierre, M., et al. 2016, AAP, 592, A1
Plotkin, R. M., Markoff, S., Kelly, B. C., Körding, E., & Anderson, S. F. 2012, MNRAS, 419, 267
Portegies Zwart, S. F., Baumgardt, H., Hut, P., Makino, J., & McMillan, S. L. W. 2004, Nature, 428, 724
Reed, S. L., et al. 2015, MNRAS, 454, 3952

Reines, A. E., & Deller, A. T. 2012, ApJ, 750, L24
Reines, A. E., Greene, J. E., & Geha, M. 2013, ApJ, 775, 116
Reines, A. E., Sivakoff, G. R., Johnson, K. E., & Brogan, C. L. 2011, Nature, 470, 66
Reines, A. E., & Volonteri, M. 2015, ApJ, 813, 82
Reines, A. E., et al. 2014, ApJ, 787, L30
Reines, A., et al. 2016, e-prints (arXiv:1610.01598)
Roche, N., et al. 2012, MNRAS, 420, 1764
Sartori, L. F., et al. 2015, MNRAS, 454, 3722
Satyapal, S., et al. 2014, ApJ, 784, 113
Schmidt, M., Schneider, D. P., & Gunn, J. E. 1995, AJ, 110, 68
Schramm, M., et al. 2013, ApJ, 773, 150
Secrest, N. J., et al. 2015, ApJ, 798, 38
Seth, A., Agüeros, M., Lee, D., & Basu-Zych, A. 2008, ApJ, 678, 116
Seth, A. C., et al. 2010, ApJ, 714, 713
Shanks, T., et al. 2015, MNRAS, 451, 4238
Shirazi, M., & Brinchmann, J. 2012, MNRAS, 421, 1043
Smidt, J., Wiggins, B. K., & Johnson, J. L. 2016, ApJL, 829, L6
Smith, A., Bromm, V., & Loeb, A. 2016, MNRAS, 460, 3143
Sobral, D., et al. 2015, ApJ, 808, 139
Stern, D., et al. 2012, ApJ, 753, 30
Stone, N. C., Kuepper, A. H. W., & Ostriker, J. P. 2016, e-prints (arXiv:1606.01909)
Thornton, C. E., Barth, A. J., Ho, L. C., Rutledge, R. E., & Greene, J. E. 2008, ApJ, 686, 892
Treister, E., Schawinski, K., Volonteri, M., & Natarajan, P. 2013, ApJ, 778, 130
Tremaine, S., et al. 2002, ApJ, 574, 740
Trichas, M., et al. 2012, ApJS, 200, 17
Ueda, Y., Akiyama, M., Hasinger, G., Miyaji, T., & Watson, M. G. 2014, ApJ, 786, 104
Utsumi, Y., et al. 2010, ApJ, 721, 1680
Valluri, M., Ferrarese, L., Merritt, D., & Joseph, C. L. 2005, ApJ, 628, 137
van den Bosch, R. C. E., & de Zeeuw, P. T. 2010, MNRAS, 401, 1770
van der Marel, R. P., Alves, D. R., Hardy, E., & Suntzeff, N. B. 2002, AJ, 124, 2639
van der Marel, R. P., Cretton, N., de Zeeuw, P. T., & Rix, H.-W. 1998, ApJ, 493, 613
van Wassenhove, S., Volonteri, M., Walker, M. G., & Gair, J. R. 2010, MNRAS, 408, 1139
Vaughan, S., Iwasawa, K., Fabian, A. C., & Hayashida, K. 2005, MNRAS, 356, 524
Venemans, B. P., et al. 2013, ApJ, 779, 24
Venemans, B. P., et al. 2015, ApJ, 801, L11
Verolme, E. K., et al. 2002, MNRAS, 335, 517
Vito, F., et al. 2013, MNRAS, 428, 354
Vito, F., et al. 2014, MNRAS, 445, 3557
Vito, F., et al. 2016, MNRAS, 463, 348
Volonteri, M. 2010, A&A Rev., 18, 279
Volonteri, M., Callegari, S., Colpi, M., Dotti, M., & Mayer, L. 2008a, MmSAI, 79, 1231
Volonteri, M., Lodato, G., & Natarajan, P. 2008b, MNRAS, 383, 1079
Volonteri, M., & Natarajan, P. 2009, MNRAS, 400, 1911
Volonteri, M., & Reines, A. E. 2016, ApJ, 820, L6
Volonteri, M., Silk, J., & Dubus, G. 2015, ApJ, 804, 148
Wang, R., et al. 2013, ApJ, 773, 44
Weigel, A. K., et al. 2015, MNRAS, 448, 3167
Whalen, T. J., et al. 2015, ApJ, 806, 37
Willott, C. J. 2011, ApJ, 742, L8
Willott, C. J., et al. 2007, AJ, 134, 2435
Willott, C. J., et al. 2009, AJ, 137, 3541
Willott, C. J., et al. 2010a, AJ, 140, 546
Willott, C. J., et al. 2010b, AJ, 139, 906
Wrobel, J. M., & Ho, L. C. 2006, ApJ, 646, L95
Wu, X.-B., et al. 2015, Nature, 518, 512
Wyithe, J. S. B., & Loeb, A. 2012, MNRAS, 425, 2892
Xiao, T., et al. 2011, ApJ, 739, 28
Xue, Y. Q., et al. 2011, ApJS, 195, 10
Xue, Y. Q., et al. 2012, ApJ, 758, 129
Yoon, Y., et al. 2015, ApJ, 808, 96